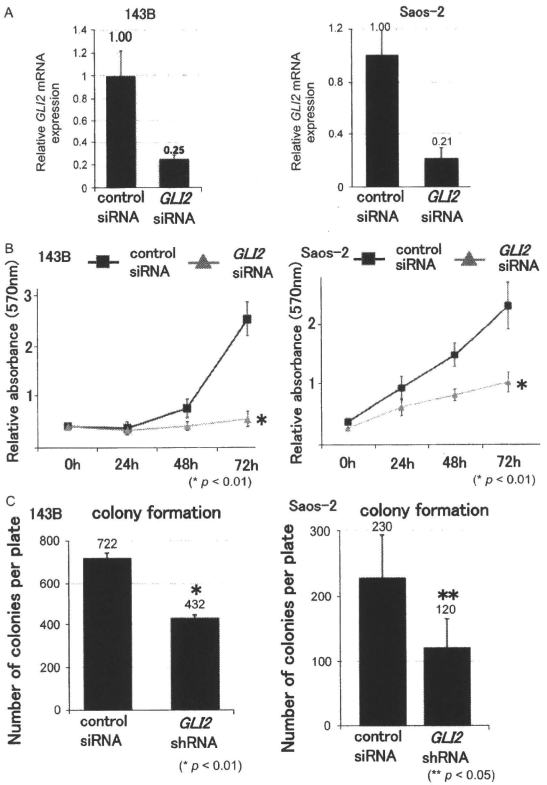

Figure 3. *GLI2* knockdown inhibits proliferation of osteosarcoma cells. (A) Transfection of *GLI2* siRNA resulted in a >70% knockdown efficiency of GLI2 [error bars represent mean (SD)]. $^{\Delta\Delta}$ Ct analysis was performed to evaluate the fold change in *GLI2* mRNA expression, using *GAPDH* or *ACTB*. (B) Growth at 72 h of 143B and Saos-2 cells was inhibited by *GLI2* siRNA. The experiment was performed in triplicate with similar results (* $p < 0.01$) [error bars represent mean (SD)]. (C) A reduced number of colonies was observed in soft agar following *GLI2* knockdown. These experiments were performed in triplicate with similar results (* $p < 0.01$; ** $p < 0.05$) [error bars represent mean (SD)].

between the osteosarcoma and prostate cancer cells *in vivo*. Nonetheless, these two studies independently suggest that low-molecular-weight compounds can inhibit malignant tumours *in vitro*. Moreover, these findings suggest that other GLI-specific inhibitors may have a powerful therapeutic potential for the management of osteosarcoma and other malignancies characterized by constitutive activation of the Hedgehog signalling pathway.

For *in vivo GLI2* RNA interference studies, we inoculated 143B osteosarcoma cells that had been previously transfected with *GLI2* shRNA. Although knockdown of *GLI2* by shRNA significantly inhibited osteosarcoma growth in nude mice, this method is not clinically applicable. Recently, the potential clinical usefulness of RNA interference in mammalian cells has been demonstrated, with no reported interferon activation [25]. In addition, Davis *et al* [26] reported a human phase I clinical trial involving the systemic administration of siRNA to patients with solid cancers; they demonstrated that siRNA administered systemically to a human can inhibit a specific gene. These findings strongly suggest that administration of *GLI2* siRNA might be a promising new treatment for osteosarcoma.

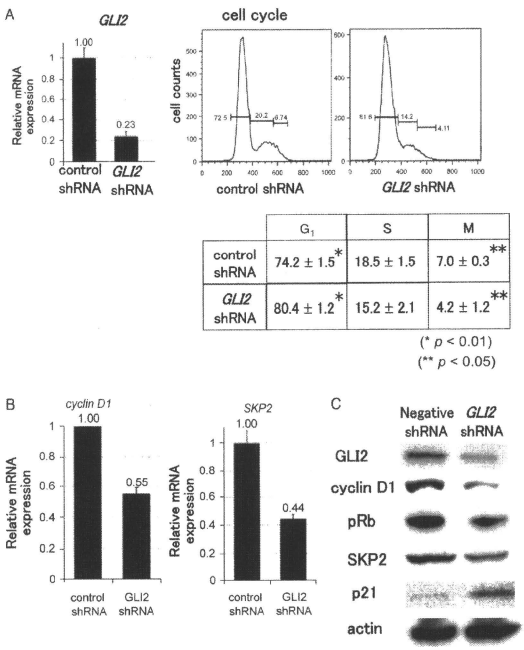

	G_1	S	M
control shRNA	74.2 ± 1.5*	18.5 ± 1.5	7.0 ± 0.3**
GLI2 shRNA	80.4 ± 1.2*	15.2 ± 2.1	4.2 ± 1.2**

(* $p < 0.01$)
(** $p < 0.05$)

Figure 4. Knockdown of *GLI2* promotes cell cycle arrest in the G_1 phase. (A) Following transfection of *GLI2* shRNA, the efficacy of *GLI2* knockdown was >75%. $^{\Delta\Delta}$ Ct analysis was performed to evaluate the fold change in mRNA expression, using *GAPDH* or *ACTB*. (B) When 143B cells were transfected with control shRNA, 74.2% of them were in G_1 phase, while when they were transfected with *GLI2* shRNA, 80.4% of the cells were in G_1 phase (*$p < 0.01$; **$p < 0.05$). (B) Real-time PCR was employed to examine the expression of cell cycle-related genes. $^{\Delta\Delta}$ Ct analysis was performed to evaluate fold changes of mRNA expression, using *GAPDH* or *ACTB*. Knockdown of *GLI2* decreased the expression of the cell cycle accelerators, *cyclin D1* and *SKP2* [error bars represent mean (SD)]. (C) Western blot analysis revealed that knockdown of *GLI2* decreased the protein levels of cyclin D1, pRb and SKP2. Western blot analysis revealed that knockdown of *GLI2* increased the expression of $p21^{Cip1}$, a negative regulator of cell cycle progression.

We previously reported that inhibition of SMO by cyclopamine or by *SMO* RNA interference reduced the growth of osteosarcoma via cell cycle regulation [21]. Compared to several potential mutational targets within the Hedgehog pathway downstream of SMO already discovered, the group of tumours that would benefit from direct GLI inhibition is substantial and likely to increase. For instance, it has been reported that inhibition of GLI, but not SMO, induced apoptosis in chronic lymphocytic leukaemia cells [27].

In order to examine the molecular mechanisms of GLI2 up-regulation, we examine genomic amplification of the GLI2 locus. We performed cytogenetic studies in three osteosarcoma specimens. FISH analysis using specific probes for the GLI2 locus revealed no chromosomal abnormalities in our osteosarcoma biopsy tissues (data not shown); this region of the genome is known to be amplified in some tumour specimens [28–32]. Further examinations should be done to elucidate the molecular mechanisms of GLI2 up-regulation.

We showed that knockdown of *GLI2* decreased the expression of SKP2 [33,34]. In addition, we found that knockdown of *GLI2* increased the expression of $p21^{Cip1}$. SKP2 is a subunit of the SCF^{SKP2} complex, a ubiquitin-dependent ligase. Down-regulation of the SCF^{SKP2} complex may promote a cell cycle arrest in G_1 phase by inhibition of $p21^{Cip1}$ degradation. Several key signalling pathways, including Hedgehog, TGFβ, BMP, Notch and Wnt, are engaged in essential processes of embryonic development. Recently, it has been clarified that these pathways also play important roles in the pathogenesis of malignant tumours (reviewed in [35]). In addition, it has been shown that there is a direct interaction or crosstalk among these key pathways (reviewed in [36]). We previously reported that

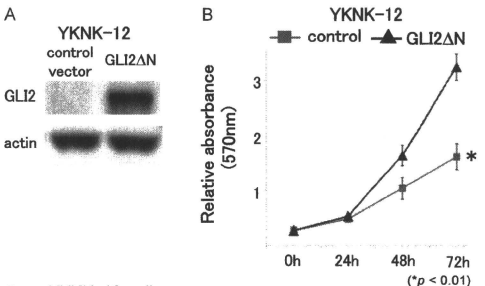

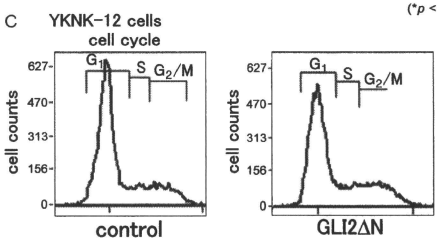

	G_1	S	M
control vector	72.0 ± 0.5*	9.8 ± 1.1**	17.0 ± 1.3*
GLI2ΔN	62.9 ± 0.9*	12.5 ± 1.0**	22.9 ± 1.5*

(*$p < 0.01$)
(**$p < 0.05$)

Figure 5. Over-expression of GLI2 accelerates mesenchymal stem cell proliferation. (A) Western blot analysis revealed that cells transfected with the GLI2ΔN expression vector reacted positively with the anti-GLI2 antibody. (B) We assessed the proliferation of YKNK-12 cells following transfection with the GLI2ΔN expression vector, which exhibits a potent transcriptional activity. The MTT assay showed that forced expression of GLI2ΔN promoted YKNK-12 cell proliferation to a greater extent than transfection with control vector (*$p < 0.01$) [error bars represent mean (SD)]. (C) Cell cycle analysis of YKNK-12 cell revealed that 62.9% and 72.0% of the cells were in G_1 phase following forced expression of GLI2ΔN and transfection with control vector, respectively. Furthermore following forced expression of GLI2ΔN, 12.5% and 22.9% of the cells were in the S and G_2–M phase, respectively, whereas 9.8% and 17.0% of the control vector-transfected cells were in the S and G_2–M phase, respectively (*$p < 0.01$; **$p < 0.05$).

the Notch pathway is activated in human osteosarcoma and that its activation promotes osteosarcoma cell growth [37]. In turn, activation of the Notch pathway promotes transcription of SKP2. SKP2 might thus mediate the crosstalk between the Notch and Hedgehog pathways. Further studies are needed to elucidate the role of interaction between these pathways in the pathogenesis of osteosarcoma.

Several recent studies have demonstrated that the anti-tumour effects of Hedgehog pathway inhibitors are mediated by their effects on tumour stromal cells [38,39]. Other studies have demonstrated that Hedgehog pathway inhibitors directly affect cancer cells [21,22,40–44]. Our findings showed that both GLI inhibition and *GLI2* knockdown directly inhibit osteosarcoma cell growth. Further studies are needed to establish the role of GLI2 activation in response to paracrine and autocrine Hedgehog signalling in osteosarcoma cells.

The hypothesis that malignant tumours are generated by rare populations of tumour-initiating cells (TICs), also called cancer stem cells, that are more tumourigenic than other cancer cells, has gained increasing credence [22,45]. We and others have reported that some bone and soft tissue sarcomas are generated by TICs [16,46]. The Hedgehog pathway has been implicated in the maintenance of normal stem cell or progenitor cells in many tissues, including the epithelia of many internal organs and brain [47]. Magali *et al* [48,49] reported that inhibition of Hedgehog

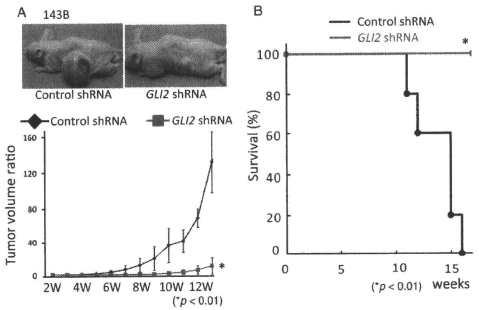

Figure 6. *GLI2* knockdown inhibits osteosarcoma growth in nude mice. (A) Following transfection of control shRNA or *GLI2* shRNA, 1×10^6 143 B cells were subcutaneously inoculated in nude mice. Tumour size was calculated weekly by using the formula $LW^2/2$ (where L and W represent the length and width of tumours). Seven days after inoculation, tumour volume was set as 1 and the increase in tumour volume was calculated at different time points, using the above formula. *GLI2* shRNA-transfected cells demonstrated a significant inhibition of tumour growth as compared with control shRNA-transfected cells ($n = 6$; $^*p < 0.01$) [error bars represent mean (SD)]. Kaplan–Meier analysis revealed that knockdown of *GLI2* provided a significant survival benefit ($n = 6$; $^*p < 0.01$).

signalling depletes TICs, whereas constitutive activation of Hedgehog signalling increases the number of TICs and accelerates tumour progression. These findings suggest that inhibition of the Hedgehog pathway might decrease the proportion of osteosarcoma TICs. The presence of a high aldehyde dehydrogenase (ALDH) activity has been used to identify TICs in malignant tumours [50–52]. Recently, Wang *et al* [53] reported that TICs obtained from osteosarcoma can be identified by a high ALDH activity. In this regard, we determined the proportion of cells with a high ALDH activity following *GLI2* siRNA transfection. At baseline, 30.6% of 143B cells showed a high ALDH activity. Seven days after *GLI2* siRNA transfection, there was no change in the proportion of cells with a high ALDH activity (data not shown). Further studies are needed to determine the impact of Hedgehog pathway inhibition on the proportion of TICs in other osteosarcoma cell lines or using other methodologies to identify TICs. In conclusion, our findings demonstrate that inhibition of GLI2 prevents osteosarcoma growth. These finding improves our understanding of osteosarcoma pathogenesis and suggest that inhibitions of GLI2 may be regarded as an effective treatment for patients with osteosarcoma.

Acknowledgment

We are grateful to Hui Gao for excellent technical assistance. We thank Dr Naoya Kobayashi (Department of Surgery, Okayama University Graduate School of Medicine and Dentistry, Japan) for providing the YKNK-12 cell line. We thank H Sasaki (Laboratory for Embryonic Induction, RIKEN Centre for Developmental Biology, Kobe, Japan) for providing the reporter vectors. This work was supported by Grants-in-Aid for Scientific Research (KAKENHI) (B) 18390419, (C) 19591725, (C) 20591786, (C) 21591919, (C) 21591920, and (C) 22591663 and a Grant-in-Aid from the Ministry of Health, Labour, and Welfare of Japan for the Third Term Comprehensive Control Research for Cancer.

Author contributions

NH, IY, NS, KS and ST conceived and designed the experiments. NH, HM, YT and TT performed the experiments. IK, NK, KS and ST analysed the data. NH and HM contributed reagents/materials/analysis tools. ST drafted the manuscript.

References

1. Sweetnam R. Osteosarcoma. *Br J Hosp Med* 1982; **28**: ,116 112–121.
2. Dorfman HD, Czerniak B. Bone cancers. *Cancer* 1995; **75**: 203–210.
3. Wu PK, Chen WM, Chen CF, *et al*. Primary osteogenic sarcoma with pulmonary metastasis: clinical results and prognostic factors in 91 patients. *Japan J Clin Oncol* 2009; **39**: 514–522.
4. Iwamoto Y, Tanaka K, Isu K, *et al*. Multi-institutional phase II study of neoadjuvant chemotherapy for osteosarcoma (NECO study) in Japan: NECO-93J and NECO-95J. *J Orthop Sci* 2009; **14**: 397–404.
5. Meyers PA, Schwartz CL, Krailo M, *et al*. Osteosarcoma: a randomized, prospective trial of the addition of ifosfamide and/or muramyl tripeptide to cisplatin, doxorubicin, and high-dose methotrexate. *J Clin Oncol* 2005; **23**: 2004–2011.
6. Kager L, Zoubek A, Kastner U, *et al*. Skip metastases in osteosarcoma: experience of the Cooperative Osteosarcoma Study Group. *J Clin Oncol* 2006; **24**: 1535–1541.
7. Horowitz JM, Park SH, Bogenmann E, *et al*. Frequent inactivation of the retinoblastoma anti-oncogene is restricted to a subset of human tumor cells. *Proc Natl Acad Sci USA* 1990; **87**: 2775–2779.

8. Ingham PW, McMahon AP. Hedgehog signaling in animal development: paradigms and principles. *Genes Dev* 2001; **15**: 3059–3087.
9. Ruiz i Altaba A, Sanchez P, Dahmane N. Gli and hedgehog in cancer: tumours, embryos and stem cells. *Nat Rev* 2002; **2**: 361–372.
10. Lum L, Beachy PA. The Hedgehog response network: sensors, switches, and routers. *Science (NY)* 2004; **304**: 1755–1759.
11. Bijlsma MF, Spek CA, Peppelenbosch MP. Hedgehog: an unusual signal transducer. *Bioessays* 2004; **26**: 387–394.
12. Ding Q, Motoyama J, Gasca S, *et al*. Diminished sonic hedgehog signaling and lack of floor plate differentiation in *Gli2* mutant mice. *Development (Camb UK)* 1998; **125**: 2533–2543.
13. Ruiz i Altaba A, Mas C, Stecca B. The *Gli* code: an information nexus regulating cell fate, stemness and cancer. *Trends Cell Biol* 2007; **17**: 438–447.
14. Nakahara H, Misawa H, Hayashi T, *et al*. Bone repair by transplantation of hTERT-immortalized human mesenchymal stem cells in mice. *Transplantation* 2009; **88**: 346–353.
15. Hijioka H, Setoguchi T, Miyawaki A, *et al*. Up-regulation of Notch pathway molecules in oral squamous cell carcinoma. *Int J Oncol* 2010; **36**: 817–822.
16. Hirotsu M, Setoguchi T, Matsunoshita Y, *et al*. Tumour formation by single fibroblast growth factor receptor 3-positive rhabdomyosarcoma-initiating cells. *Br J Cancer* 2009; **101**: 2030–2037.
17. Sasaki H, Hui C, Nakafuku M, *et al*. A binding site for Gli proteins is essential for HNF-3β floor plate enhancer activity in transgenics and can respond to Shh *in vitro*. *Development (Camb. UK)* 1997; **124**: 1313–1322.
18. Sasaki H, Nishizaki Y, Hui C, *et al*. Regulation of Gli2 and Gli3 activities by an amino-terminal repression domain: implication of Gli2 and Gli3 as primary mediators of Shh signaling. *Development (Camb, UK)* 1999; **126**: 3915–3924.
19. Fukushima M, Setoguchi T, Komiya S, *et al*. Retinal astrocyte differentiation mediated by leukemia inhibitory factor in cooperation with bone morphogenetic protein 2. *Int J Dev Neurosci* 2009; **27**: 685–690.
20. Sasaki H, Setoguchi T, Matsunoshita Y, *et al*. The knock-down of over-expressed EZH2 and BMI-1 does not prevent osteosarcoma growth. *Oncology Rep* 2010; **23**: 677–684.
21. Hirotsu M, Setoguchi T, Sasaki H, *et al*. Smoothened as a new therapeutic target for human osteosarcoma. *Mol Cancer* 2010; **9**: 5.
22. Lauth M, Bergstrom A, Shimokawa T, *et al*. Inhibition of GLI-mediated transcription and tumor cell growth by small-molecule antagonists. *Proc Natl Acad Sci USA* 2007; **104**: 8455–8460.
23. Tang N, Song WX, Luo J, *et al*. Osteosarcoma development and stem cell differentiation. *Clin Orthop Rel Res* 2008; **466**: 2114–2130.
24. Roessler E, Ermilov AN, Grange DK, *et al*. A previously unidentified amino-terminal domain regulates transcriptional activity of wild-type and disease-associated human *GLI2*. *Hum Mol Genet* 2005; **14**: 2181–2188.
25. Elbashir SM, Harborth J, Lendeckel W, *et al*. Duplexes of 21-nucleotide RNAs mediate RNA interference in cultured mammalian cells. *Nature* 2001; **411**: 494–498.
26. Davis ME, Zuckerman JE, Choi CH, *et al*. Evidence of RNAi in humans from systemically administered siRNA via targeted nanoparticles. *Nature* 2010; **464**: 1067–1070.
27. Desch P, Asslaber D, Kern D, *et al*. Inhibition of GLI, but not Smoothened, induces apoptosis in chronic lymphocytic leukemia cells. *Oncogene* 2010; **29**: 4885–4895.
28. Gimenez S, Costa C, Espinet B, *et al*. Comparative genomic hybridization analysis of cutaneous large B-cell lymphomas. *Exp Dermatol* 2005; **14**: 883–890.
29. Fishman A, Shalom-Paz E, Fejgin M, *et al*. Comparing the genetic changes detected in the primary and secondary tumor sites of ovarian cancer using comparative genomic hybridization. *Int J Gynecol Cancer* 2005; **15**: 261–266.
30. Liu XP, Sato T, Oga A, *et al*. Two subtypes of mucinous colorectal carcinoma characterized by laser scanning cytometry and comparative genomic hybridization. *Int J Oncol* 2004; **25**: 615–621.
31. Wreesmann VB, Ghossein RA, Hezel M, *et al*. Follicular variant of papillary thyroid carcinoma: genome-wide appraisal of a controversial entity. *Genes Chromosomes Cancer* 2004; **40**: 355–364.
32. Wei G, Lonardo F, Ueda T, . *et al*. *CDK4 gene amplification in osteosarcoma: reciprocal relationship with INK4A gene alterations and mapping of 12q13 amplicons*. *Int J Cancer* 1999; **80**: 199–204.
33. Kamura T, Hara T, Matsumoto M, *et al*. Cytoplasmic ubiquitin ligase KPC regulates proteolysis of p27(Kip1) at G_1 phase. *Nat Cell Biol* 2004; **6**: 1229–1235.
34. Hara T, Kamura T, Kotoshiba S, *et al*. Role of the UBL-UBA protein KPC2 in degradation of p27 at G_1 phase of the cell cycle. *Mol Cell Biol* 2005; **25**: 9292–9303.
35. Rubin LL, de Sauvage FJ. Targeting the Hedgehog pathway in cancer. *Nat Rev Drug Discov* 2006; **5**: 1026–1033.
36. Ross J, Li L. Recent advances in understanding extrinsic control of hematopoietic stem cell fate. *Curr Opin Hematol* 2006; **13**: 237–242.
37. Tanaka M, Setoguchi T, Hirotsu M, *et al*. Inhibition of Notch pathway prevents osteosarcoma growth by cell cycle regulation. *Br J Cancer* 2009; **100**: 1957–1965.
38. Tian H, Callahan CA, DuPree KJ, *et al*. Hedgehog signaling is restricted to the stromal compartment during pancreatic carcinogenesis. *Proc Natl Acad Sci USA* 2009; **106**: 4254–4259.
39. Yauch RL, Gould SE, Scales SJ, *et al*. A paracrine requirement for hedgehog signalling in cancer. *Nature* 2008; **455**: 406–410.
40. Sanchez P, Hernandez AM, Stecca B, *et al*. Inhibition of prostate cancer proliferation by interference with sonic hedgehog–GLI1 signaling. *Proc Natl Acad Sci USA* 2004; **101**: 12561–12566.
41. Singh RR, Cho-Vega JH, Davuluri Y, *et al*. Sonic hedgehog signaling pathway is activated in ALK-positive anaplastic large cell lymphoma. *Cancer Res* 2009; **69**: 2550–2558.
42. Lindemann RK. Stroma-initiated hedgehog signaling takes center stage in B-cell lymphoma. *Cancer Res* 2008; **68**: 961–964.
43. Wong SY, Seol AD, So PL, *et al*. Primary cilia can both mediate and suppress Hedgehog pathway-dependent tumorigenesis. *Nat Med* 2009; **15**: 1055–1061.
44. Dierks C, Beigi R, Guo GR, *et al*. Expansion of *Bcr-Abl*-positive leukemic stem cells is dependent on Hedgehog pathway activation. *Cancer Cell* 2008; **14**: 238–249.
45. Clarke MF, Fuller M. Stem cells and cancer: two faces of Eve. *Cell* 2006; **124**: 1111–1115.
46. Murase M, Kano M, Tsukahara T, *et al*. Side population cells have the characteristics of cancer stem-like cells/cancer-initiating cells in bone sarcomas. *Br J Cancer* 2009; **101**: 1425–1432.
47. Beachy PA, Karhadkar SS, Berman DM. Tissue repair and stem cell renewal in carcinogenesis. *Nature* 2004; **432**: 324–331.
48. Dierks C, Grbic J, Zirlik K, *et al*. Essential role of stromally induced hedgehog signaling in B-cell malignancies. *Nat Med* 2007; **13**: 944–951.
49. Zhao C, Chen A, Jamieson CH, *et al*. Hedgehog signalling is essential for maintenance of cancer stem cells in myeloid leukaemia. *Nature* 2009; **458**: 776–779.
50. Ginestier C, Hur MH, Charafe-Jauffret E, *et al*. ALDH1 is a marker of normal and malignant human mammary stem cells and a predictor of poor clinical outcome. *Cell Stem Cell* 2007; **1**: 555–567.
51. Huang EH, Hynes MJ, Zhang T, *et al*. Aldehyde dehydrogenase 1 is a marker for normal and malignant human colonic stem cells

(SC) and tracks SC overpopulation during colon tumorigenesis. *Cancer Res* 2009; **69**: 3382–3389.

52. Cheung AM, Wan TS, Leung JC, *et al*. Aldehyde dehydrogenase activity in leukemic blasts defines a subgroup of acute myeloid leukemia with adverse prognosis and superior NOD/SCID engrafting potential. *Leukemia* 2007; **21**: 1423–1430.

53. Wang L, Park P, Zhang H, *et al*. Prospective identification of tumorigenic osteosarcoma cancer stem cells in OS99–1 cells based on high aldehyde dehydrogenase activity. *Int J Cancer* 2011; **128**: 294–303.

SUPPORTING INFORMATION ON THE INTERNET

The following supporting information may be found in the online version of this article:

Figure S1. Knockdown of GLI2 promotes cell arrest of Saos-2 cell.

See related Commentary on page 2166

The American Journal of Pathology, Vol. 177, No. 5, November 2010

DOI: 10.2353/ajpath.2010.100134

Cell Injury, Repair, Aging and Apoptosis

Stromal Cell-Derived Factor-1 Is Essential for Photoreceptor Cell Protection in Retinal Detachment

Hiroki Otsuka,* Noboru Arimura,* Shozo Sonoda,* Makoto Nakamura,† Teruto Hashiguchi,‡ Ikuro Maruyama,‡ Shintaro Nakao,§ Ali Hafezi-Moghadam,§ and Taiji Sakamoto*

From the Departments of Ophthalmology, and Laboratory and Vascular Medicine,† Kagoshima University Graduate School of Medical and Dental Sciences, Kagoshima, Japan; the Division of Ophthalmology, the Department of Surgery, Kobe University Graduate School of Medicine, Kobe, Japan; and the Angiogenesis Laboratory,§ Massachusetts Eye and Ear Infirmary, the Department of Ophthalmology, Harvard Medical School, Boston, Massachusetts*

Stromal cell-derived factor-1 (SDF-1) causes chemotaxis of CXCR4-expressing bone marrow-derived cells. SDF-1 is involved in the pathogenesis of various vascular diseases, including those of the eye. However, the role of SDF-1 in neuronal diseases is not completely understood. Here, we show higher SDF-1 levels in the vitreous humor of patients with retinal detachment (RD) compared with normal patients. SDF-1 correlated positively with the duration as well as the extent of RD. Furthermore, SDF-1 correlated significantly with levels of interleukin-6 and interleukin-8, but not with vascular endothelial growth factor. Western blot analysis results showed significant SDF-1 up-regulation in detached rat retinas compared with normal animals. Immunohistochemistry data showed that SDF-1 was co-localized with the glial cells of the detached retina. SDF-1 blockade with a neutralizing antibody increased photoreceptor cell loss and macrophage accumulation in the subretinal space. The retinal precursor cell line R28 expressed CXCR4. SDF-1 rescued serum starvation-induced apoptosis in R28 cells and enhanced their ability to participate in wound closure in a scratch assay. Our results indicate a surprising, protective role for SDF-1 in RD. This effect may be mediated directly or indirectly through other cell types. ***(Am J Pathol 2010, 177:2268–2277; DOI: 10.2353/ajpath.2010.100134)***

Chemokines are a family of polypeptides that act as potent chemoattractants. They are structurally grouped into two subfamilies, CXC-family and CC- subfamily, based on the characteristic presence of four conserved cysteine residues.[1–3] Stromal cell-derived factor-1 (SDF-1) is a CXC-chemokine with important roles in hematopoiesis.[4] Mice lacking SDF-1 or its receptor CXCR4 are embryonically lethal, exhibiting defects in various organs including heart, brain, large vessels, and bone marrow.[5,6] In bone marrow, endothelial cells and stromal cells express SDF-1, which not only recruits hematopoietic stem cells to the bone marrow niche, but also supports their survival and proliferation.[7,8] SDF-1/CXCR4 also recruits bone marrow-derived cells to neovascularization and regeneration sites in heart, liver,[9,10] and eye.[11,12]

SDF-1 levels are elevated in the vitreous of ischemic ocular diseases, such as proliferative diabetic retinopathy (PDR) and retinopathy of prematurity.[12,13] Previously, we reported elevated vitreous levels of SDF-1 in patients with retinal vein occlusion.[14] In addition, SDF-1/CXCR4 potentially mediates ocular inflammation by recruiting $CD4^+$ T-cells, and is potentially involved in the formation of proliferative membranes in eyes with proliferative vitreoretinopathy.[15,16] Therefore, interest in understanding the role of SDF-1/CXCR4 in non-neovascular inflammatory or proliferative ocular diseases remains great.

Retinal detachment (RD), the physical separation of the neural layer of the retina from the subjacent retinal pigment epithelium, results in photoreceptor cell death.[17,18] Because of the irreversible nature of the damage, a long duration of RD can cause permanent vision loss.[19] Thus, new insights into the photoreceptor protection in RD would be of great clinical interest, as they could lead to new treatments. Because, the retina is an acces-

Supported in part by a grant from the Research Committee on Chorioretinal Degeneration and Optic Atrophy, Ministry of Health, Labor, and Welfare (T.S.), and by a Grant-in-Aid for Scientific Research (number 20390450) from the Ministry of Education, Science, and Culture of the Japanese Government.

Accepted for publication June 24, 2010.

CME Disclosure: None of the authors disclosed any relevant financial relationships.

Address reprint requests to Taiji Sakamoto, M.D., Ph.D., Department of Ophthalmology, Kagoshima University Graduate School of Medical and Dental Sciences, 8-35-1, Sakuragaoka, Kagoshima, 890-8520, Japan. E-mail: tsakamot@m3.kufm.kagoshima-u.ac.jp.

sible part of the brain, it also offers a unique opportunity for studies of the central nervous system. Given that RD usually occurs without infectious inflammation or destructive ischemia, it provides a suitable context for investigating morphological changes in neural disorders and a local sterile inflammation.

The CC chemokine monocyte chemotactic protein-1, erythropoietin, and interleukin (IL)-6 have recently been implicated in neuro protection.[20,21] Monocyte chemotactic protein-1 is a critical mediator of RD-induced photoreceptor apoptosis.[22]

This study elucidates the role of SDF-1 in RD by using human vitreous samples *in vivo* and *in vitro*.

Materials and Methods

Human Vitreous Samples

This study was approved by the institutional ethical committee at University of Kagoshima, and was performed in accordance with the Declaration of Helsinki. All surgeries were performed at Kagoshima University Hospital. All patients provided informed consent before receiving treatment. Undiluted vitreous fluid samples (0.5 to 0.7 ml) were obtained from the same sites of the anterior vitreous by pars plana vitrectomy. Vitreous humor was collected in sterile tubes, placed immediately on ice, centrifuged to remove cells and debris, and stored at −80°C until analysis. The clinical histories of all patients were obtained from their medical records. In patients with rhegmatogenous RD (RRD), preoperative data collection included time from onset of symptoms to surgery and extent of detached retina.

Measurements of vitreous levels of SDF-1α, vascular endothelial growth factor (VEGF), and inflammatory cytokines/chemokines (IL-1β, IL-6, IL-8, IL-10, IL-12p70, and tumor necrosis factor-α) were measured as we described previously.[23] SDF-1α and VEGF were quantified by using commercial enzyme-linked immunosorbent assays (Human CXCL12/SDF-1 α Quantikine ELISA Kit, Human VEGF Quantikine ELISA Kit; R&D Systems, Minneapolis, MN). Six inflammatory cytokines/chemokines were quantified by using commercial multiplex Cytometric Bead Array systems: Human Inflammation Kit (BD Biosciences Pharmingen, San Diego, CA). All concentrations less than the detection level were assigned a value of 0 in the subsequent analysis.

Animals and RD Induction

All experiments were performed in accordance with the Association for Research in Vision and Ophthalmology statement for the Use of Animals in Ophthalmic and Vision Research and approval of our institutional animal care committee. Brown Norway rats (Kyudo, Fukuoka, Japan), postnatal 8 weeks, were studied as follows. RD was induced in the right eyes as we described previously.[23] The rats were anesthetized with an intramuscular injection of ketamine and xylazine, and their pupils were dilated with topical 1% tropicamide and 2.5% phenylephrine hydrochloride. The retinas were detached by using a subretinal injection of 1% sodium hyaluronate (Opegan; Santen, Osaka, Japan) with an anterior chamber puncture to reduce intraocular pressure. Sclera was penetrated at the ocular nasal equator with a 30-Gauge needle. Then, sodium hyaluronate (0.05 ml) was gently injected through the sclera into the subretinal space to enlarge the RDs. These procedures were performed only in the right eye, with the left eye serving as a control. Eyes with lens injury, vitreous hemorrhage, infection, and spontaneous reattachment were excluded from the analysis.

Intravitreal Injection

In some eyes, immediately after RD induction, 1 μg anti-SDF-1α antibody (MAB310; R&D Systems) or 1 μg isotype control IgG1 monoclonal antibody (MAB002; R&D Systems) was injected intravitreally from the temporal limbus of the same eye by using a 33-Gauge needle (Hamilton, Reno, NV) in a 10-μl volume. Doses were based on previous studies in mice.[24] The rats were sacrificed on days 3 and 7 after treatment, and the eyes were harvested for study.

Western Blot Analysis of Experimental RD

SDF-1 expression in the detached retinas was examined by Western blot, as described previously.[25] The rats were sacrificed 3 days after RD induction. The eyes were enucleated immediately, and the anterior segment and vitreous were removed. The detached portion of the neurosensory retina was carefully peeled and harvested. Retinas were resuspended in lysis buffer (30 mmol/L Tris, pH 7.5, 150 mmol/L NaCl, 1 mmol/L phenylmethylsulfonyl fluoride, 1 mmol/L Na3VO4, 1% Nonidet P-40, and 10% grycerol), and centrifuged for 10 minutes at 4°C. Protein concentration in the supernatant was calculated by using the micro bicinchoninic acid protein assay kit (Pierce, Rockford, IL). An aliquot of 50 μg total extract was mixed with protein loading buffer containing methoxyethanol, and boiled for 5 minutes before being loaded onto 15% SDS-polyacrylamide gels, then transferred onto a polyvinylidene difluoride membrane. The membrane was blocked by incubation with blocking buffer (Tris-buffered saline [pH 7.5] with 5% nonfat dry milk and 0.1% Tween-20) for 1 hour at room temperature. The membrane was then incubated with rabbit polyclonal anti-SDF-1α antibody (1:1000; Abcam, Cambridge, UK) at 4°C overnight. The blots were subsequently probed with secondary anti-rabbit antibodies conjugated to horseradish peroxidase, and images were developed by using the enhanced chemiluminescence system plus (GE Health care, Tokyo, Japan).

Immunofluorescent Staining

The eyes were fixed in 4% paraformaldehyde at 4°C overnight. The anterior segment and the lens were removed, and the remaining eye cup was cryoprotected with 10% to 30% sucrose in PBS. The eye cups were then frozen in an optimal cutting temperature compound (Sakura Finetech, Tokyo, Japan). Frozen sections (8 μm) were dried and

blocked with blocking buffer for 1 hour. The antibodies used for staining were rabbit polyclonal anti-SDF-1α antibody, rabbit polyclonal anti-CXCR4 antibody (each 1:50; Abcam), monoclonal anti-glial fibrillary acidic protein (GFAP) antibody (Sigma, St. Louis, MO), mouse anti-CD68 monoclonal antibody (ED1; 1:800; Serotec, Raleigh, NC), and mouse anti-CD31 monoclonal antibody (PECAM-1; 1:100; Abcam). Normal rabbit or mouse IgG was used instead of primary antibody as a negative control in each case. Secondary antibodies were Alexa-Fluor 488-conjugated goat anti-mouse IgG $F(ab)_2$ fragment and Alexa-Fluor 594-conjugated goat anti-rabbit IgG $F(ab)_2$ fragment (each 1:400; Molecular Probes, Carlsbad, CA). Slides were counterstained with 4,6-diamidino-2-phenylindole (DAPI), mounted with Shandon PermaFlour (Thermo Scientific, Waltham, MA), and viewed with a Olympus fluorescence microscope (Olympus, Tokyo, Japan). Images were captured by using the same exposure time for each comparative section. Confocal Laser Scanning Microscopy images were taken on an Olympus FV-500 confocal microscope (Olympus). For all experiments, at least three sections from each eye were evaluated.

Immunofluorescent staining for CXCX4 was performed on R28 cells by using the same method.

Quantification of Outer Nuclear Layer Thickness and ED1 Positive Macrophages

To evaluate the change of outer nuclear layer (ONL) thickness after RD, we compared the thickness of the ONL with the entire retina (defined as the distance between the internal limiting membrane to the external limiting membrane) in histological sections (three sections each point) stained with hematoxylin and eosin. Three separate measurements of retinal thickness were obtained from each retinal section by using image analysis software, Image J (National Institutes of Health, Bethesda, MD). To assess the number of ED1 positive macrophages infiltrating the subretinal space, we performed double immune-fluorescence staining with rabbit polyclonal anti-CXCR4 antibody and ED1. The number of ED1 positive cells was counted at three random fields in each eye in a masked fashion.

Cell Culture

The rat immortalized retinal precursor cell line R28, a gift from Dr. G. M. Siegel (The State University of New York, Buffalo), was cultured in Dulbecco's modified Eagle's medium high glucose supplemented with 10% fetal bovine serum, 10 mmol/L nonessential amino acids, and 10 mg/ml gentamicin as described previously.[26] Cells were incubated at 37°C in a 5% CO_2 incubator and subcultured with 0.05% trypsin-EDTA. Subconfluent cultures were trypsinized and seeded for the following experiments.

Trypan Blue Dye Exclusion Assay

To induce cell death by serum starvation, R28 cells at 50% confluence in 24-well tissue culture plates were washed with PBS twice, and the culture medium was replaced with serum-free Dulbecco's modified Eagle's medium containing 0.1% bovine serum albumin. After 6 hours of synchronization, recombinant SDF-1α (PeproTech, London, UK) or PBS was added to the wells at the indicated concentrations. After incubation for 48 hours, cell survival was assessed by trypan blue dye exclusion assay in a masked fashion, as described previously.[27]

Terminal Deoxynucleotidyl Transferase-Mediated dUTP Nick-End Labeling Staining

Terminal deoxynucleotidyl transferase-mediated dUTP nick-end labeling (TUNEL) procedure and quantification of TUNEL-positive cells were performed by using an ApopTag fluorescein direct *in situ* apoptosis detection kit (Chemicon International, Temecula, CA) according to the manufacturer's instructions. The number of TUNEL-positive cells was counted in a masked fashion.

Scratch Wound Assay

For scratch wound assay, R28 cells were grown to 90% confluence in 6-well tissue culture plates and serum starved for 6 hours before experiment. Then, R28 cells were scratched with a sterile 0.1- to 10-μl pipette tip (TipOne; USA Scientific, Ocala, FL) to remove cells with three parallel linear scrapes. The debris of damaged cells was removed by washing, and the cells were refed with serum-free Dulbecco's modified Eagle's medium containing 0.1% bovine serum albumin in the presence or absence of recombinant (rSDF-1) (100 ng/ml). The progression of wound healing was photographed immediately and 24 hours after wounding, at the same field near the marked point, using an inverted microscope (Olympus CKX41; Olympus) equipped with a digital camera. The extent of healing is defined as the ratio of the area difference between the original wound and the remaining wound 24 hours after injury compared with the original wound.[28] The wound area was determined by the number of pixels in histogram (Photoshop CS3; Adobe, San Jose, CA).

Western Blot Analysis of Bcl-2 or ERK-1/2 Activation

R28 cells (5×10^5) were subcultured on 6-cm tissue culture dishes. The cells were serum-starved for 6 hours and then stimulated with or without rSDF-1 (100 ng/ml) for 24 hours.[29] For inhibition studies, U0126 (Promega, Madison, WI) was added 1 hour before SDF-1 treatment. In brief, whole cells were lysed with SDS sample buffer and a 80-μg volume of protein extracts was loaded onto 15% SDS-polyacrylamide gels, then transferred onto a polyvinylidene difluoride membrane. After blocking, the membrane was reacted with anti-Bcl-2 antibody (1:1000; Cell Signaling Technology, Beverly, MA) at 4°C overnight. The blots were subsequently probed with secondary antibodies and images were developed. To analyze activation of ERK-1/2, the membrane was reacted with phospho-ERK-

Table 1. Patient Characteristics

Characteristics	PDR	RRD	ERM	MH	*P*
Subjects, no.	30	44	11	18	
Age (yr)	62 (31–80)	59 (44–86)	69 (50–75)	68 (49–78)	0.184*
Female sex no. (%)	15 (50)	18 (41)	6 (55)	11 (61)	0.849†

Values are expressed as the median (range) or number (%).
*Kruskal-Wallis variance analysis.
†χ^2 test.

1/2 (1:1000; Cell Signaling Technology). After detection of phospho-ERK-1/2, the blot was stripped and re-probed with an antibody against total ERK-1/2 (1:1000; Cell Signaling Technology), as described previously.[30]

Statistical Analysis

The vitreous inflammatory cytokine/chemokine concentrations in each group were compared by using the Mann-Whitney *U*-test. The correlation between inflammatory cytokines/chemokines in RD samples was analyzed by using a simple linear regression analysis and Spearman's rank correlation coefficient. All *in vitro* and vivo data are presented as mean ± SEM, and the significance of differences between groups was determined by Student's *t*-test. *P* values less than 0.05 were considered significant.

Results

Vitreous SDF-1 and Inflammatory Cytokine/Chemokine Levels in Patients with RD, Epiretinal Membrane, and Macular Hole

To investigate the role of SDF-1 in non-neovascular ocular diseases, we quantified the levels of human vitreous SDF-1 in RRD, epiretinal membrane (ERM), and macular hole (MH). PDR, a neovascular disease with high levels of SDF-1 in the vitreous, was used as a positive control.[31] Samples were harvested from 30 eyes with PDR, 44 eyes with RRD, 11 eyes with ERM, and 18 eyes with MH. There were no statistically significant differences in age and sex of patients (Table 1).

SDF-1 concentration of RRD (58.5 pg/ml) was significantly higher than that of ERM (21.2 pg/ml, $P = 0.012$ and $P < 0.016$ after Bonferroni correction). Significant differences were not found between RRD and MH (10.0 pg/ml), or between MH and ERM (Figure 1A). The vitreous VEGF level in PDR was highest and comparable to that of SDF-1. In contrast, there was surprisingly no VEGF detectable in RRD, ERM, and MH (Figure 1B).

Next, we examined whether there is a relation between vitreous SDF-1 concentration and pathological condition in eyes with RRD, in terms of duration of disease (range, 3 to 120 days) and extent of detached retina (range, 0.5 to 4 quadrants; Table 2). The vitreous SDF-1 level in RRD was positively correlated with duration of disease and extent of detached retina in RRD by a simple linear regression ($r = 0.501$, $P < 0.001$, $r = 0.339$, $P = 0.024$, respectively) and by a Spearman's rank correlation coefficient ($r = 0.347$, $P = 0.025$, $r = 0.323$, $P = 0.040$, respectively; Figure 1, C and D).

Furthermore, vitreous SDF-1 showed a positive correlation with IL-6 ($r = 0.484$, $P = 0.002$) and IL-8 ($r = 0.400$, $P = 0.009$) by Spearman's rank correlation coefficient (Figure 1, E and F), but not by simple linear regression. The vitreous IL-6 in RRD positively correlated with the extent of detached retina by a Spearman's rank correlation coefficient ($r = 0.342$, $P = 0.027$; data not shown); however, it did not correlate with disease duration.

SDF-1 and CXCR4 Expression in Experimental RD

To investigate SDF-1 and CXCR4 expression in the retina after RD, 3 days after detachment was induced in Brown Norway rats, neurosensory retina was harvested and expression of these proteins was analyzed by Western blotting. The SDF-1 protein level in the detached retina was substantially higher ($P < 0.01$), 3 days after RD, compared with the untreated control (Figure 2, A and B).

Immunofluorescent staining revealed sparse SDF-1 expression in the inner border and the outer plexiform layer of the retina in the control. In contrast, up-regulation of the expression of SDF-1 occurred with RD (Figure 3, A and B), which seemed to be colocalized with the activated GFAP-positive astrocytes or Müller cells (Figure 3, C–F).

In the normal retina, CXCR4 staining mainly was present in the ganglion cell layer and the inner nuclear layer of the retina. Additionally, CXCR4 was strongly positive in the outer nuclear layer and photoreceptor inner segments of the detached retina (Figure 4, A–D). Double immunofluorescent staining of CXCR4 showed strong staining in some ED-1-positive macrophages infiltrating into the subretinal space (Figure 5, A–C).

Vitreal SDF-1 Neutralization Causes ONL Cell Loss and Accumulation of Subretinal ED-1 Positive Macrophages

To further define the role of SDF-1 in RD, after sodium hyaluronate injection into the subretinal space, some rats were intravitreally injected with anti-SDF-1 antibody or nonbinding control antibody. Three days after RD, there were no apparent morphological differences between the Ab-injected animals and normal controls. Seven days after RD, there was thinning of the outer nuclear layer due

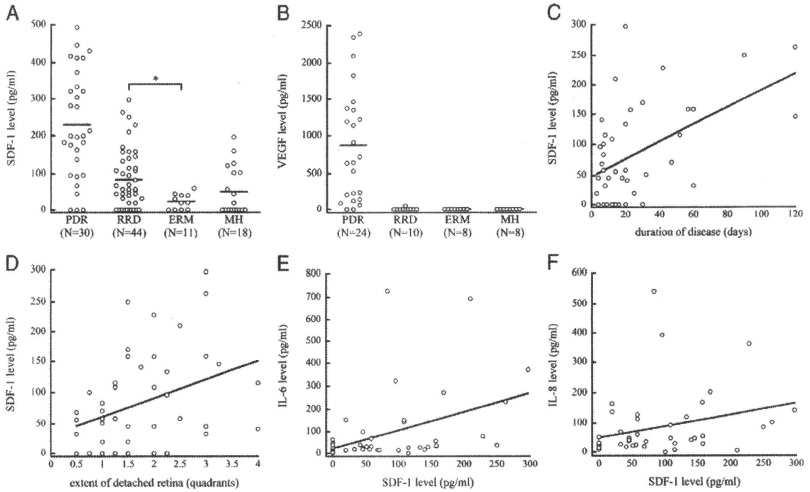

Figure 1. Analysis of human vitreous levels of SDF-1. **A:** Vitreous levels of PDR, RRD, ERM, and MH. The vitreous SDF-1 level of RRD was significantly higher than that of ERM. Bars indicate average values. **B:** Vitreous levels of VEGF. **C** and **D:** Scatter plot for the correlation between vitreous levels of SDF-1 and (**C**) duration of disease (simple linear regression, $r = 0.501$, $P < 0.001$; Spearman's rank correlation coefficient, $r = 0.347$, $P = 0.025$) or (**D**) extent of detached retina (simple linear regression, $r = 0.339$, $P = 0.024$; Spearman's rank correlation coefficient, $r = 0.323$, $P = 0.040$) in eyes with RRD. **E** and **F:** Scatter plot for the correlation between vitreous levels of SDF-1 and (**E**) IL-6 (simple linear regression, $r = 0.410$, $P = 0.006$; Spearman's rank correlation coefficient, $r = 0.484$, $P = 0.002$) or (**F**) IL-8 duration of disease (simple linear regression, $r = 0.081$, $P = 0.061$; Spearman's rank correlation coefficient, $r = 0.400$, $P = 0.009$) in eyes with RRD.

to photoreceptor loss and deconstruction of the inner and outer segments of the photoreceptors. The ratio of the thickness of the ONL to the entire retina differed significantly between the noninjected (0.278 ± 0.015) and anti-SDF-1 Ab group (0.228 ± 0.011, $P < 0.05$), or between anti-SDF-1 Ab and control Ab group (0.294 ± 0.018, $P < 0.01$), respectively. No significant difference was found between noninjected and control Ab group (Figure 6, A and B). In normal eyes without detachment, SDF-1 blockade did not cause apparent retinal morphological change (data not shown). This suggests that SDF-1 blockade results in photoreceptor cell loss only at the site of detachment.

TUNEL staining of rat eyes 3 days after detachment revealed significantly higher percentages of TUNEL-positive cells in the ONL of retinas treated with anti-SDF-1 Ab compared with those treated with control Ab ($P < 0.05$) or untreated control ($P < 0.05$; Figure 6, C and D).

To assess the impact of SDF-1 blockade on the recruitment of inflammatory cells, the number of infiltrated macrophages was counted after immunostaining with ED-1. The number of ED-1 positive macrophages that infiltrated the subretinal space was markedly increased in anti-SDF-1 Ab group, compared with both noninjected ($P < 0.05$) and control Ab group ($P < 0.05$; Figure 6, E and F).

Table 2. Clinical State of Rhegmatogenous Retinal Detachment

Duration of disease (days)	15 (3–120)
Extent of detached retina (quadrants)	1.5 (0.5–4)

Values are expressed as the median (range).

SDF-1/CXCL12 Enhances R28 Survival and Apoptosis

To assess whether SDF-1 is a survival factor for retinal cells, we performed *in vitro* experiments with R28 cells, a

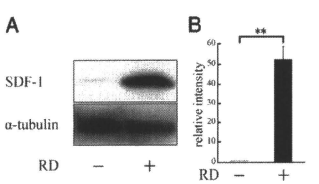

Figure 2. Western blot analysis of SDF-1 protein expression in retinas of normal rats and 3 days after detachment. Experimental retinal detachment was created by injection of sodium hyaluronate. The neurosensory retina was harvested and analyzed by Western blotting. **A:** Immunoreactive band for SDF-1 in rat retinal tissue with or without detachment. **B:** Quantification of the relative SDF-1 expression ($n = 3$). Results are the mean ± SEM. $^{**}P < 0.01$.

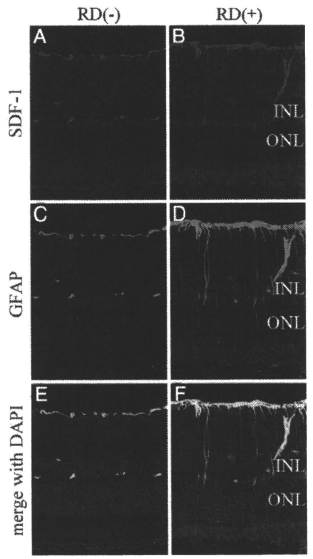

Figure 3. Confocal images of SDF-1 expression in detached rat retina. Retinal sections from control eyes (**A**, **C**, and **E**) or 3 days after detachment (**B**, **D**, and **F**). **A:** Untreated control, showing some immunofluorescent staining in the inner border and the outer plexiform layer of the retina. **B:** Three days after detachment, SDF-1 was also expressed radially, in the border of inner retina, and some nonspecific staining was found in the photoreceptor outer segment. **C** and **D:** GFAP staining. **E** and **F:** Merged image of SDF-1 (red), GFAP (green), and DAPI (blue). Colocalization of SDF-1 and GFAP was found regardless of RD, but stronger in detached retina compared with control. INL, internal nuclear layer; ONL, outer nuclear layer. Original magnifications, ×200.

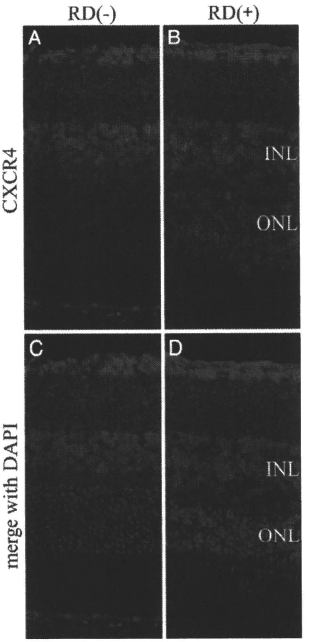

Figure 4. Confocal images of CXCR4 expression in detached rat retina. The retinal sections were derived from control eyes (**A** and **C**) or 3 days after detachment (**B** and **D**). **A:** Untreated control retina, showing positive staining in the ganglion cell layer and the inner nuclear layer of the retina. **B:** Three days after detachment, CXCR4 was strongly positive in the outer nuclear layer and photoreceptor inner segments of the detached retina. **C** and **D:** Merged images of CXCR4 (red) and DAPI (blue). INL, internal nuclear layer; ONL, outer nuclear layer. Original magnifications, ×200.

rat retinal progenitor cell line.[32,33] Cell surface expression of CXCR4 was found by immunofluorescent staining (Figure 7A). To induce cell apoptosis, we first cultured R28 cells under serum-starvation with or without SDF-1, and assessed cell survival by trypan blue dye exclusion assay after 48 hours of culturing. Serum starvation for 48 hours caused a 36.1% reduction of cell survival, compared with serum-containing medium. SDF-1 treatment dose dependently rescued serum starvation-induced cell death by 19.1% at 100 ng/ml rSDF-1 ($P < 0.05$, Figure 7B). The effect of SDF-1 was completely reversed by treatment with anti-SDF-1 antibodies (1 μg/ml; Figure 7B). TUNEL staining revealed that 11.8 ± 6.1% of cells were apoptotic after 48 hours of serum starvation. By contrast, treatment with SDF-1 significantly reduced the frequency of TUNEL-positive cells (6.5 ± 5.2%, $P < 0.05$; Figure 7, C and D). Less than 1% of the cells were TUNEL-positive with serum-containing medium. These results indicate that SDF-1 inhibits the apoptosis induced by serum starvation in R28 cells.

SDF-1 Increases Wound Healing

To study the effects of SDF-1 on wound healing, we performed a scratch wound healing assay in the presence of SDF-1. The 90% confluent monolayers of R28

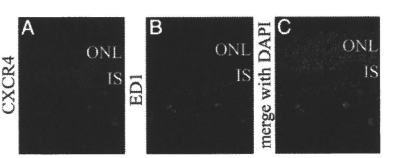

Figure 5. CXCR4 is expressed in the macrophages infiltrating into subretinal space. The retinal sections were derived at 3 days after detachment. **A:** CXCR4 staining was positive in the macrophages infiltrating into subretinal space. **B:** ED-1 stained macrophages in subretinal space. **C:** Merged image of CXCR4 (red), ED1 (green), and DAPI (blue). ONL, Outer nuclear layer; IS, inner segment. Original magnifications, ×400.

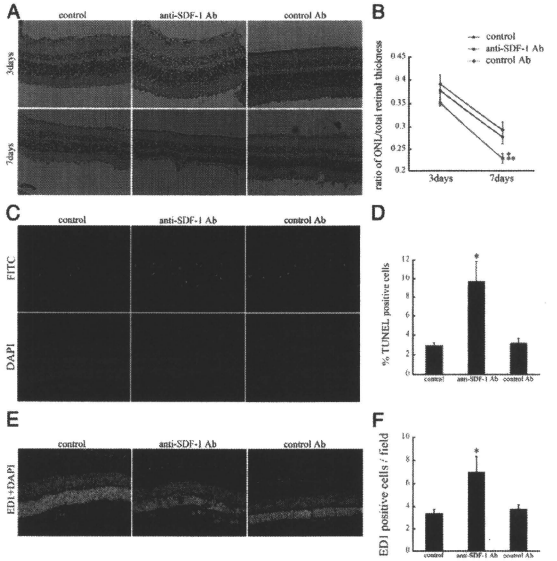

Figure 6. Effect of SDF-1 inhibition on retinal ONL thickness. Anti-SDF-1 Ab or control Ab was intravitreally injected immediately after RD induction. The rats without intravitreal injections served as controls. **A:** No apparent morphological differences among the three groups, 3 days after RD. By day 7 after RD, ONL thickness in anti-SDF-1 Ab-injected eyes was significantly lower compared with normal controls or control Ab-injected eyes. Original magnifications, ×200. **B:** Graph summarizing effects of intravitreal injection on ONL thickness of rat retinas at 3 and 7 days after detachment. Results are the mean ± SEM. $*P < 0.05$; control Ab versus anti-SDF-1 Ab injection at day 7. $**P < 0.01$; control versus anti-SDF-1 Ab injection at day 7. **C:** TUNEL staining (green) and DAPI (blue) of detached rat retinas treated with anti-SDF-1 Ab or control Ab at day 3 after RD. **D:** Quantification of TUNEL-positive cells in ONL among three groups. Results are the mean ± SEM. $*P < 0.05$; control versus anti-SDF-1 antibody injection. **E:** Immunofluorescent staining for ED1 (green) and DAPI (blue) showing infiltrated cells into the subretinal space at day 7 after RD. Original magnifications, ×200. **F:** Quantification of the number of ED-1-positive macrophages among the three groups. Results are the mean ± SEM, $*P < 0.01$; control versus anti-SDF-1 antibody injection.

cells were scratched by using a pipette tip to create a wound area. The wound area was photographed after the scratch and 24 hours later, while the cells were kept in serum-free media, containing 0.1% bovine serum albumin in the presence or absence of rSDF-1 (100 ng/ml; Figure 8A). Subsequently, the dimensions of the healing areas were calculated (Figure 8B).

SDF-1 treatment significantly increased wound closure by 24.2% compared with control ($P < 0.01$). SDF-1's effect was reduced by the addition of anti-

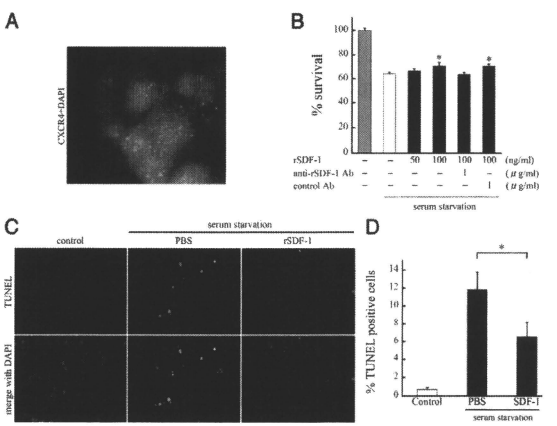

Figure 7. SDF-1 supports R28 cell survival suppressing serum starvation-induced apoptosis. **A:** Double immunofluorescent staining of CXCR4 (green) and DAPI (blue) of R28 cells. CXCR4 was predominantly expressed on the cell surface. Original magnifications, ×1000. **B:** The effect of SDF-1 on cell survival. R28 cells were serum-starved and treated with PBS or rSDF-1 at the indicated doses. After 48 hours of culture, the surviving cells were counted by trypan blue dye exclusion assay ($n = 4$ each). The effect of SDF-1 was reversed by anti-SDF-1 antibody but not by control antibody. Results are the mean ± SEM. $*P < 0.05$ versus PBS-treated control. **C** and **D:** TUNEL staining (**C**) and quantitative analysis of the TUNEL-positive apoptotic nuclei (**D**) in serum-starved R28 cells treated with PBS or rSDF-1 ($n = 4$ each). The cells growing in serum-containing medium were used as controls. Results are the mean ± SEM. $*P < 0.05$.

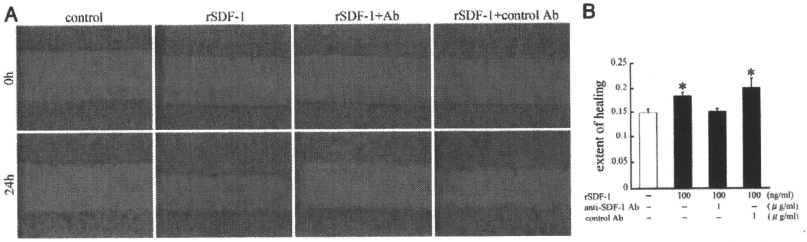

Figure 8. Effect of SDF-1 on wound healing in R28 cells. **A:** Serum-starved R28 cells at confluence were injured with a 10-μL pipette tip. Wounded cells were allowed to heal for 24 hours in the presence or absence (control) of rSDF-1 (100 ng/ml). The extent of healing was improved by SDF-1 treatment. The effect of SDF-1 was reversed by anti-SDF-1 antibody but not by control antibody. Original magnifications, ×40. **B:** Changes in the extent of healing in R28 cells. Results are the mean ± SEM. $^{*}P < 0.01$; versus control.

SDF-1 Ab (0.151 ± 0.020), but not control Ab (0.201 ± 0.019).

SDF-1 Caused Bcl-2 Up-Regulation and ERK-1/2 Phosphorylation

To investigate the cytosolic signaling involved in survival-enhancing activity of SDF-1, we performed Western blotting by using anti-Bcl-2 antibody. The R28 cells were serum-starved and cultured with or without rSDF-1 (100 ng/ml). After 24 hours of culturing, whole cell lysates were analyzed. Western blot analysis showed increased Bcl-2 protein expression in R28 cells with SDF-1 treatment ($P < 0.01$; Figure 9, A and B).

In addition, we incubated the cells with 100 ng/ml rSDF-1 after 6 hours of serum starvation, and examined activation of signaling molecules by Western blotting by using phosphospecific antibodies. SDF-1 treatment of the R28 cells caused rapid activation of ERK1/2, which was statistically significant starting at 15 minutes ($P < 0.01$; Figure 9, C and D). The blockade of ERK signaling pathway by U0126 caused a significant reduction of Bcl-2 expression ($P < 0.01$; Figure 9, E and F).

Discussion

The present study shows the role of SDF-1 in non-neovascular ocular diseases. SDF-1 and its receptor, CXCR4, are highly expressed in the detached retina, and vitreal SDF-1 correlates with the RD pathology in patients. SDF-1 neutralization increases photoreceptor apoptosis after RD, indicating its surprising role in neuroprotection. *In vitro*, SDF-1 increases cell survival by reducing apoptosis and improving cell migration. To our knowledge, this is the first report showing increased intraocular levels of SDF-1 and its critical role in photoreceptor survival in RD.

SDF-1 has received widespread attention for its involvement in VEGF-associated ocular neovascularization, and neuroprotection through the recruitment of bone marrow-derived cells.[9,24] For example, SDF-1 and VEGF positively correlate in diabetic retinopathy.[31] Such a correlation was also found in the PDR eyes of the present study, confirming the role of SDF-1 in the PDR pathogenesis. Previously, Butler et al[12] reported that SDF-1 is necessary and sufficient to promote proliferative retinopathy. In contrast, despite high SDF-1, significant neovas-

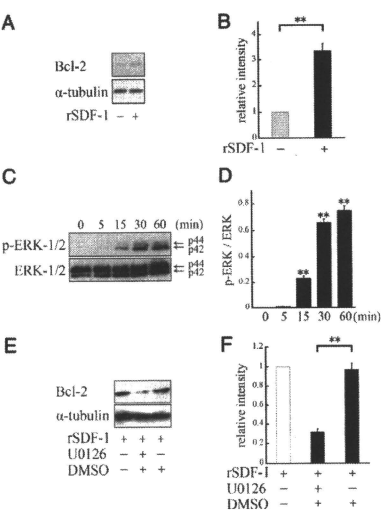

Figure 9. A: SDF-1 induced up-regulation of Bcl-2 protein expression. R28 cells were serum-starved and cultured with rSDF-1 (100 ng/ml) for 24 hours, and total cell lysates were analyzed by Western blot. **B:** Quantification of the relative expression of Bcl-2. Results are representative of three independent experiments, expressed as the mean ± SEM. $^{**}P < 0.01$. **C:** SDF-1 induced the phosphorylation of ERK. R28 cells were stimulated with rSDF-1 (100 ng/ml) for 5, 15, 30, or 60 minutes. **D:** Quantification of p-ERK/ERK ratio. Results are representative of three independent experiments, expressed as the mean ± SEM. $^{**}P < 0.01$; versus control. **E:** ERK signaling was essential to the regulation of Bcl-2. After 3 hours of serum starvation, U0126 was applied 1 hour before SDF-1 treatment. **F:** Quantification of the relative expression of Bcl-2. $^{**}P < 0.01$; versus dimethyl sulfoxide.

cularization or proliferative retinopathy was not found in our RD eyes.[12] Our results indicate that SDF-1 alone is not sufficient to promote proliferative retinopathy, suggesting that in addition to high SDF-1, VEGF, ischemic injury, or other factors might be necessary to promote proliferative retinopathy in humans. The positive correlation of SDF-1 with disease duration, as well as the extent of the detached retina, indicates that SDF-1 is produced by the detached retina or a related event. SDF-1 was also positively correlated with IL-6, a protective factor in RD,[21] suggesting that part of SDF-1's action might be through other factors. These clinical data indicate SDF-1 to be a key player in RD pathology.

In our study, although RD shows the highest vitreous SDF-1 levels among the studied conditions, VEGF levels in RD are low. However, considering outer retinal ischemia,[34] the VEGF level was also expected to be high. Possible explanations of this discrepancy are as follows: (1) there are undetectable levels of VEGF production; (2) VEGF is released predominantly into subretinal space in RD. Further studies will be required to elucidate this point.

In ocular diseases, SDF-1 is induced by ischemia.[35,36] Retinal glia,[35] as well as endothelial cells, releases SDF-1.[36] SDF-1 colocalizes in the inner retina with GFAP expressing cells in normal and detached retinas, suggesting SDF-1 production in glial cells, such as Müller cells, astrocytes, and microglias. Up-regulation of GFAP positive glia is found in relation to central nervous system stress, including RD.[37,38] Therefore, it appears likely that SDF-1 is released by reactive retinal glia in RD. In RD, the inner retina is believed to be sufficiently supplied by retinal circulation so that ischemia generally does not occur,[34] suggesting that other stimuli besides ischemia might be responsible for SDF-1 up-regulation.

SDF-1 blockade causes a significant accumulation of inflammatory cells in the subretinal space and photoreceptor loss after RD. This is in line with the finding that SDF-1 blockade aggravates retinal degeneration in C3H/HeJ (rd1/rd1) mice.[24] SDF-1 rescues serum starvation-induced apoptosis of R28 cells dose-dependently, possibly through bcl2 up-regulation and activation of the ERK-pathway. This is in line with a previous report that SDF-1 suppresses apoptosis of cultured dendritic cells.[39]

SDF-1 stimulates the wound-healing response in R28 cells. Because SDF-1 is up-regulated both in the animal model of RD and in samples from patients with RD, it is reasonable to assume that SDF-1 is part of the organ's response to minimize injury, and that blocking it would enhance retinal damage.

Sasahara et al[24] reported that SDF-1 blockade decreases the accumulation of neuro-protective bone marrow-derived microglial cells, resulting in progression of retinal degeneration. Our results show accumulation of CXCR4-positive macrophages around the retinal vessels and in the subretinal spaces, suggesting that SDF-1 acts as a chemo-attractant for inflammatory cells in RD. However, accumulation of subretinal macrophages increased significantly in the SDF-1-blocked eyes, differing from the results by Sasahara et al[24] in the retinal degeneration model. An explanation for this discrepancy could be that in RD, the retina is damaged acutely and more severely than in the chronic retinal degeneration model. As a result, the mediators of cell damage might differ between RD and retinal degeneration. For instance, damage-associated molecular pattern molecules, strong chemo-attractants for inflammatory cells, are produced after injury,[40,41] and we found the damage-associated molecular pattern molecule member, the high-mobility group box-1, subretinally in RD.[23]

The fact that SDF-1 blockade increases damage in detached retinas suggests that SDF-1 might limit the production of chemical mediators of injury, including damage-associated molecular pattern molecules. This might also explain the increased accumulation of inflammatory cells in the subretinal space of RD eyes with SDF-1 blockade.

Interestingly, SDF-1 blockade affects the detached but not the normal retina, suggesting that the detached-retina is more sensitive to environmental changes than the normal retina. This tendency was also described in RD of IL-6$^{-/-}$ mice.[21] SDF-1 blockade has been proposed as a new therapeutic strategy for proliferative ocular diseases.[12] However, proliferative diseases are often associated with RD, so anti-SDF-1 therapy might be counter-indicated.

Anti-VEGF agents have recently shown therapeutic success in age-related macular degeneration and diabetic retinopathy.[42] Intraocular mediators of inflammation and angiogenesis build a complex network, and targeting one of them affects various others. We showed that VEGF inhibition decreases SDF-1 in the eye.[23] This might explain some of the deleterious effects of anti-VEGF therapy and indicate the need for careful consideration of the indication for VEGF-targeting with respect to RD.

In sum, SDF-1 has both beneficial and adverse effects in RD, such as neuro-protection or inflammatory cell accumulation, respectively. Endogenous SDF-1 is tissue-protective in RD. Elucidating the detailed mechanisms underlying SDF-1's role in neural protection will support the development of safe and effective treatments.

References

1. Schall TJ: Biology of the RANTES/SIS cytokine family. Cytokine 1991, 3:165–183
2. Oppenheim JJ, Zachariae CO, Mukaida N, Matsushima K: Properties of the novel proinflammatory supergene "intercrine" cytokine family. Annu Rev Immunol 1991, 9:617–648
3. Luster AD: Chemokines–chemotactic cytokines that mediate inflammation. N Engl J Med 1998, 338:436–445
4. Schall TJ, Bacon KB: Chemokines, leukocyte trafficking, and inflammation. Curr Opin Immunol 1994, 6:865–873
5. Nagasawa T, Hirota S, Tachibana K, Takakura N, Nishikawa S, Kitamura Y, Yoshida N, Kikutani H, Kishimoto T: Defects of B-cell lymphopoiesis and bone-marrow myelopoiesis in mice lacking the CXC chemokine PBSF/SDF-1. Nature 1996, 382:635–638
6. Lazarini F, Tham TN, Casanova P, Arenzana-Seisdedos F, Dubois-Dalcq M: Role of the alpha-chemokine stromal cell-derived factor (SDF-1) in the developing and mature central nervous system. Glia 2003, 42:139–148
7. Burger JA, Kipps TJ: CXCR4: a key receptor in the crosstalk between tumor cells and their microenvironment. Blood 2006, 107:1761–1767

8 Tataillade JJ, Clay D, Dupuy C, Rigal S, Jasmin C, Bourin P, Le Bousse-Kerdiles MC: Chemokine SDF-1 enhances circulating CD34(+) cell proliferation in synergy with cytokines: possible role in progenitor survival. Blood 2000, 95:756–768
9. Ruiz de Almodovar C, Luttun A, Carmeliet P: An SDF-1 trap for myeloid cells stimulates angiogenesis. Cell 2006, 124:18–21
10 Askari AT, Unzek S, Popovic ZB, Goldman CK, Forudi F, Kiedrowski M, Rovner A, Ellis SG, Thomas JD, DiCorleto PE, Topol EJ, Penn MS: Effect of stromal-cell-derived factor 1 on stem-cell homing and tissue regeneration in ischaemic cardiomyopathy. Lancet 2003, 362:697–703
11 Sengupta N, Caballero S, Mames RN, Butler JM, Scott EW, Grant MB: The role of adult bone marrow-derived stem cells in choroidal neovascularization. Invest Ophthalmol Vis Sci 2003, 44:4908–4913
12. Butler JM, Guthrie SM, Koc M, Afzal A, Caballero S, Brooks HL, Mames RN, Segal MS, Grant MB, Scott EW: SDF-1 is both necessary and sufficient to promote proliferative retinopathy. J Clin Invest 2005, 115:86–93
13. Sonmez K, Drenser KA, Capone A Jr, Trese MT: Vitreous levels of stromal cell-derived factor 1 and vascular endothelial growth factor in patients with retinopathy of prematurity. Ophthalmology 2008, 115:1065–1070
14 Ki IY, Arimura N, Noda Y, Yamakiri K, Doi N, Hashiguchi T, Maruyama I, Shimura M, Sakamoto T: Stromal-derived factor-1 and inflammatory cytokines in retinal vein occlusion. Curr Eye Res 2007, 32:1065–1072
15. Curnow SJ, Wloka K, Faint JM, Amft N, Cheung CM, Savant V, Lord J, Akbar AN, Buckley CD, Murray PI, Salmon M: Topical glucocorticoid therapy directly induces up-regulation of functional CXCR4 on primed T lymphocytes in the aqueous humor of patients with uveitis. J Immunol 2004, 172:7154–7161
16. Abu El-Asrar AM, Struyf S, Kangave D, Geboes K, Van Damme J: Chemokines in proliferative diabetic retinopathy and proliferative vitreoretinopathy. Eur Cytokine Netw 2006, 17:155–165
17. Cook B, Lewis GP, Fisher SK, Adler R: Apoptotic photoreceptor degeneration in experimental retinal detachment. Invest Ophthalmol Vis Sci 1995, 36:990–996
18. Yang L, Bula D, Arroyo JG, Chen DF: Preventing retinal detachment-associated photoreceptor cell loss in Bax-deficient mice. Invest Ophthalmol Vis Sci 2004, 45:648–654
19. Arroyo JG, Yang L, Bula D, Chen DF: Photoreceptor apoptosis in human retinal detachment. Am J Ophthalmol 2005, 139:605–610
20. Digicaylioglu M, Lipton SA: Erythropoietin-mediated neuroprotection involves cross-talk between Jak2 and NF-kappaB signalling cascades. Nature 2001, 412:641–647
21. Chong DY, Boehlke CS, Zheng QD, Zhang L, Han Y, Zacks DN: Interleukin-6 as a photoreceptor neuroprotectant in an experimental model of retinal detachment. Invest Ophthalmol Vis Sci 2008, 49:3193–3200
22. Nakazawa T, Hisatomi T, Nakazawa C, Noda K, Maruyama K, She H, Matsubara A, Miyahara S, Nakao S, Yin Y, Benowitz L, Hafezi-Moghadam A, Miller JW: Monocyte chemoattractant protein 1 mediates retinal detachment-induced photoreceptor apoptosis. Proc Natl Acad Sci USA 2007, 104:2425–2430
23. Arimura N, Otsuka H, Yamakiri K, Sonoda Y, Nakao S, Noda Y, Hashiguchi T, Maruyama I, Sakamoto T: Vitreous mediators after intravitreal bevacizumab or triamcinolone acetonide in eyes with proliferative diabetic retinopathy. Ophthalmology 2009, 116:921–926
24. Sasahara M, Otani A, Oishi A, Kojima H, Yodoi Y, Kameda T, Nakamura H, Yoshimura N: Activation of bone marrow-derived microglia promotes photoreceptor survival in inherited retinal degeneration. Am J Pathol 2008, 172:1693–1703
25. Xie Z, Wu X, Qiu Q, Gong Y, Song Y, Gu Q, Li C: Expression pattern of erythropoietin and erythropoietin receptor in experimental model of retinal detachment. Curr Eye Res 2007, 32:757–764
26. Neekhra A, Luthra S, Chwa M, Seigel G, Gramajo AL, Kuppermann BD, Kenney MC: Caspase-8, -12, and -3 activation by 7-ketocholesterol in retinal neurosensory cells. Invest Ophthalmol Vis Sci 2007, 48:1362–1367
27 Sareen D, van Ginkel PR, Takach JC, Mohiuddin A, Darjatmoko SR, Albert DM, Polans AS: Mitochondria as the primary target of resveratrol-induced apoptosis in human retinoblastoma cells. Invest Ophthalmol Vis Sci 2006, 47:3708–3716
28. Xu KP, Yu FS: Cross talk between c-Met and epidermal growth factor receptor during retinal pigment epithelial wound healing. Invest Ophthalmol Vis Sci 2007, 48:2242–2248
29. Murakami Y, Ikeda Y, Yonemitsu Y, Onimaru M, Nakagawa K, Kohno R, Miyazaki M, Hisatomi T, Nakamura M, Yabe T, Hasegawa M, Ishibashi T, Sueishi K: Inhibition of nuclear translocation of apoptosis-inducing factor is an essential mechanism of the neuroprotective activity of pigment epithelium-derived factor in a rat model of retinal degeneration. Am J Pathol 2008, 173:1326–1338
30. Arimura N, Ki-i Y, Hashiguchi T, Kawahara K, Biswas KK, Nakamura M, Sonoda Y, Yamakiri K, Okubo A, Sakamoto T, Maruyama I: Intraocular expression and release of high-mobility group box 1 protein in retinal detachment. Lab Invest 2009, 89:278–289
31. Brooks HL Jr, Caballero S Jr, Newell CK, Steinmetz RL, Watson D, Segal MS, Harrison JK, Scott EW, Grant MB: Vitreous levels of vascular endothelial growth factor and stromal-derived factor 1 in patients with diabetic retinopathy and cystoid macular edema before and after intraocular injection of triamcinolone. Arch Ophthalmol 2004, 122:1801–1807
32. Seigel GM, Sun W, Wang J, Hershberger DH, Campbell LM, Salvi RJ: Neuronal gene expression and function in the growth-stimulated R28 retinal precursor cell line. Curr Eye Res 2004, 28:257–269
33 Seigel GM, Mutchler AL, Adamus G, Imperato-Kalmar EL: Recoverin expression in the R28 retinal precursor cell line. In Vitro Cell Dev Biol Anim 1997, 33:499–502
34. Wang S, Linsenmeier RA: Hyperoxia improves oxygen consumption in the detached feline retina. Invest Ophthalmol Vis Sci 2007, 48:1335–1341
35. Lima e Silva R, Shen J, Hackett SF, Kachi S, Akiyama H, Kiuchi K, Yokoi K, Hatara MC, Lauer T, Aslam S, Gong YY, Xiao WH, Khu NH, Thut C, Campochiaro PA: The SDF-1/CXCR4 ligand/receptor pair is an important contributor to several types of ocular neovascularization. FASEB J 2007, 21:3219–3230
36. Lai P, Li T, Yang J, Xie C, Zhu X, Xie H, Ding X, Lin S, Tang S: Upregulation of stromal cell-derived factor 1 (SDF-1) expression in microvasculature endothelial cells in retinal ischemia-reperfusion injury. Graefes Arch Clin Exp Ophthalmol 2008, 246:1707–1713
37 Nakazawa T, Takeda M, Lewis GP, Cho KS, Jiao J, Wilhelmsson U, Fisher SK, Pekny M, Chen DF, Miller JW: Attenuated glial reactions and photoreceptor degeneration after retinal detachment in mice deficient in glial fibrillary acidic protein and vimentin. Invest Ophthalmol Vis Sci 2007, 48:2760–2768
38. Lewis GP, Fisher SK: Up-regulation of glial fibrillary acidic protein in response to retinal injury: its potential role in glial remodeling and a comparison to vimentin expression. Int Rev Cytol 2003, 230:263–290
39. Hernandez-Lopez C, Valencia J, Hidalgo L, Martinez VG, Zapata AG, Sacedon R, Varas A, Vicente A: CXCL12/CXCR4 signaling promotes human thymic dendritic cell survival regulating the Bcl-2/Bax ratio. Immunol Lett 2008, 120:72–78
40. Yang D, Chen Q, Yang H, Tracey KJ, Bustin M, Oppenheim JJ: High mobility group box-1 protein induces the migration and activation of human dendritic cells and acts as an alarmin. J Leukoc Biol 2007, 81:59–66
41. Abraham E, Arcaroli J, Carmody A, Wang H, Tracey KJ: HMG-1 as a mediator of acute lung inflammation. J Immunol 2000, 165:2950–2954
42 Rosenfeld PJ, Brown DM, Heier JS, Boyer DS, Kaiser PK, Chung CY, Kim RY: Ranibizumab for neovascular age-related macular degeneration. N Engl J Med 2006, 355:1419–1431

THE JOURNAL OF IMMUNOLOGY

B Cell-Derived Vascular Endothelial Growth Factor A Promotes Lymphangiogenesis and High Endothelial Venule Expansion in Lymph Nodes

Binita Shrestha, Teruto Hashiguchi, Takashi Ito, Naoki Miura, Kazunori Takenouchi, Yoko Oyama, Ko-ichi Kawahara, Salunya Tancharoen, Yuya Ki-i, Noboru Arimura, Narimasa Yoshinaga, Satoshi Noma, Chandan Shrestha, Takao Nitanda, Shinichi Kitajima, Kimiyoshi Arimura, Masahiro Sato, Taiji Sakamoto and Ikuro Maruyama

J Immunol 2010;184;4819-4826; Prepublished online 22 March 2010;
doi:10.4049/jimmunol.0903063
http://www.jimmunol.org/content/184/9/4819

The Journal of Immunology is published twice each month by The American Association of Immunologists, Inc., 9650 Rockville Pike, Bethesda, MD 20814-3994.

Print ISSN: 0022-1767 Online ISSN: 1550-6606.

B Cell-Derived Vascular Endothelial Growth Factor A Promotes Lymphangiogenesis and High Endothelial Venule Expansion in Lymph Nodes

Binita Shrestha,*[,1] Teruto Hashiguchi,*[,1] Takashi Ito,*[,1] Naoki Miura,[†,1] Kazunori Takenouchi,* Yoko Oyama,* Ko-ichi Kawahara,* Salunya Tancharoen,* Yuya Ki-i,[‡] Noboru Arimura,[‡] Narimasa Yoshinaga,[‡] Satoshi Noma,[§] Chandan Shrestha,* Takao Nitanda,[¶] Shinichi Kitajima,[¶] Kimiyoshi Arimura,[‖] Masahiro Sato,[#] Taiji Sakamoto,[‡] and Ikuro Maruyama*

Vascular endothelial growth factor A (VEGF-A) is a prominent growth factor for both angiogenesis and lymphangiogenesis. Recent studies have shown the importance of VEGF-A in enhancing the growth of lymphatic endothelial cells in lymph nodes (LNs) and the migration of dendritic cells into LNs. VEGF-A is produced in inflamed tissues and/or in draining LNs, where B cells are a possible source of this growth factor. To study the effect of B cell-derived VEGF-A, we created transgenic mice ($CD19^{Cre}$/$hVEGF\text{-}A^{fl}$) that express human VEGF-A specifically in B cells. We found that the human VEGF-A produced by B cells not only induced lymphangiogenesis in LNs, but also induced the expansion of LNs and the development of high endothelial venules. Contrary to our expectation, we observed a significant decrease in the Ag-specific Ab production postimmunization with OVA and in the proinflammatory cytokine production postinoculation with LPS in these mice. Our findings suggest immunomodulatory effects of VEGF-A: B cell-derived VEGF-A promotes both lymphangiogenesis and angiogenesis within LNs, but then suppresses certain aspects of the ensuing immune responses. *The Journal of Immunology*, **2010, 184: 4819–4826.**

Host defense against infection requires the integrated function of both the innate and the adaptive immune systems. Innate immune responses, which represent the front line of the immune system, are elicited by a variety of cell types, including granulocytes, macrophages, mast cells, NK cells, and dendritic cells (DCs). DCs are the professional APCs that form the bridge between innate and adaptive immune responses (1). DCs process material from invading pathogens and damaged tissues, which results in the upregulation of CCR7. Expression of CCR7 allows the DCs to enter draining lymphatic vessels that express the CCR7 ligands CCL21 and CCL19 (2). On reaching the draining lymph nodes (LNs), the DCs interact with T and B cells, thus inducing adaptive immune responses.

Lymphatic vessels are essential for transporting tissue fluid, extravasated plasma proteins, and cells back to the blood circulation (3). Lymphatic vessels contribute to the immune surveillance of the body by transporting Ag-bearing DCs from peripheral tissues to the regional LNs, where they present Ags to lymphocytes. Congenital or acquired dysfunction of lymphatic vessels leads to chronic swelling, adipose degeneration, immune dysfunction, and susceptibility to infection (3).

Lymphatic vessels are not simply inert drainage ducts; rather, they are actively involved in many physiologic and pathologic processes. For example, remodeling of lymphatic vessels by tumor-derived lymphangiogenic factors actively promotes cancer metastasis (4–6). Lymphatic vessels are also remodeled in various inflammatory conditions (7), and these remodeled vessels promote inflammation (8–10). Recent studies have revealed that lymphatic vessel growth (lymphangiogenesis) is regulated by vascular endothelial growth factor (VEGF)-C and -D via their receptor, VEGFR-3 (10, 11). In addition, VEGF-A and its receptor, VEGFR-2, also play an important role in lymphangiogenesis, especially in the enlargement of lymphatic vessels (6, 12, 13).

During inflammatory conditions, remodeling of lymphatic vessels occurs not only in inflamed peripheral tissues, but also in the regional LNs. Expansion of lymphatic vessels within LNs is important because it enhances the mobilization of DCs to the draining LNs (14). Expansion of lymphatic vessels within LNs can be locally controlled by lymphangiogenic factors released within the LNs (14, 15) or remotely controlled by factors released in the peripheral tissues (16). In the former case, this process depends upon the

*Department of Laboratory and Vascular Medicine, [†]Department of Ophthalmology, and [‖]Department of Neurology and Geriatrics, Graduate School of Medical and Dental Sciences, [‡]Laboratory of Diagnostic Imaging, Department of Veterinary Medicine, Faculty of Agriculture, and [#]Section of Gene Expression Regulation, Frontier Science Research Center, Kagoshima University; and [§]Division of Respiratory Medicine, Respiratory and Stress Care Center and [¶]Division of Surgical Pathology, Kagoshima University Medical and Dental Hospital, Kagoshima, Japan

[1]B.S., T.H., T.I., and N.M. contributed equally to this work.

Received for publication September 23, 2009. Accepted for publication February 17, 2010.

This work was supported in part by Grants-in-Aid for Scientific Research from the Ministry of Education, Science and Culture of Japan (C: 17590888, C: 13670659, C: 15590901, and B: 19390156) and by a grant from Mitsubishi Pharma Research Foundation, Japan (to T.H.).

Address correspondence and reprint requests to Dr. Teruto Hashiguchi, Department of Laboratory and Vascular Medicine, Cardiovascular and Respiratory Disorders, Kagoshima University Graduate School of Medical and Dental Sciences, 8-35-1, Sakuragaoka, Kagoshima 890-8520, Japan. E-mail address: terutoha@m3.kufm.kagoshima-u.ac.jp

The online version of this article contains supplemental material.

Abbreviations used in this paper: CAG, CMV enhancer/chicken β-actin promoter; CAT, chloramphenicol acetyltransferase; DC, dendritic cell; EGFP, enhanced green fluorescent protein; HEV, high endothelial venule; hVEGF-A, human vascular endothelial growth factor A; LN, lymph node; LYVE-1, lymphatic vessel endothelial hyaluronan receptor-1; mVEGF-A: mouse vascular endothelial growth factor A; ND, not detected; p-hVEGF-A, plasmid of human vascular endothelial growth factor A; Tg, transgenic; VEGF-A, vascular endothelial growth factor A; WT, wild-type.

www.jimmunol.org/cgi/doi/10.4049/jimmunol.0903063

presence of B cells within the LNs (14, 15). B cells in inflamed LNs express VEGF-A and can be stimulated to secrete VEGF-A in vitro (14), suggesting the involvement of B cell-derived VEGF-A in lymphangiogenesis and DC mobilization. However, the exact role of B cell-derived VEGF-A in vivo is still unknown.

In this study, we investigated the effect of B cell-derived VEGF-A in vivo using $CD19^{Cre}$/hVEGF-A^{fl} mice that express human VEGF-A (hVEGF-A) specifically in B cells. We found that these mice had enlarged LNs, with expanded lymphatic vessels and increased high endothelial venules (HEVs), even when they were not immunized. To the best of our knowledge, this is the first study describing the effect of B cell-derived VEGF-A in vivo.

Materials and Methods

Mice

Mice were kept under environmentally controlled pathogen-free conditions (light from 7:00 to 19:00; water, and standard, rodent diet ad libitum; 23°C; 55% humidity). Mice of C57BL/6N background were used to generate the transgenic (Tg) mice. Mice heterozygous for Cre recombinase inserted into the *CD19* locus ($CD19^{Cre}$ mice) (17) were kindly provided by Dr. Ursula Lichtenberg, Institute for Genetics, University of Cologne, Cologne, Germany. Animal experiments were performed in accordance with the guidelines of the Frontier Science Research Center, Kagoshima University, Kagoshima, Japan. All efforts were taken to minimize the number of animals used and their suffering.

Establishment of $CD19^{Cre}$/hVEGF-A^{fl} mice

The plasmid construct, containing human *VEGF-A* flanked by second *loxP* site (p-hVEGF-A^{fl}), is shown in Fig. 1*Ai*. To construct the p-hVEGF-A^{fl}, the *lacZ* gene in pCETZ-17 (18) was replaced by the 576 bp cDNA encoding human *VEGF-A*. The resulting DNA construct (p-hVEGF-A^{fl}) contains a CMV enhancer/chicken β-actin promoter (CAG), an enhanced green fluorescent protein (EGFP)/chloramphenicol acetyltransferase (CAT) sandwiched between two *loxP* sites and human *VEGF-A* flanked by *loxP*.

The 5.4-kb SpeI fragment containing the hVEGF-A^{fl} transgene was removed from the p-hVEGF-A^{fl} vector and microinjected into the pronuclei of the fertilized eggs of C57BL/6N mice (18). The Tg founder (F0) mice (termed hVEGF-A^{fl} mice) were identified by EGFP fluorescent blood cells using flow cytometry, as EGFP fluorescence is expressed ubiquitously under the control of the CAG promoter system (19). Blood samples used for the analysis were obtained at the time of tail cut and immersed immediately into 1 ml 3.13% sodium citrate buffer.

The presence of the hVEGF-A^{fl} transgene was confirmed by PCR. All F0 Tg mice were then crossed onto wild-type (WT) C57BL/6N mice (aged 12–20 wk). $CD19^{Cre}$ mice were mated with heterozygous hVEGF-A^{fl} mice to obtain bigenic (double Tg) offspring expressing Cre in a B cell-specific manner ($CD19^{Cre}$/hVEGF-A^{fl} mice).

In vivo assay for Cre-mediated DNA recombination

In the absence of Cre, hVEGF-A expression is prevented by the intervening transcriptional EGFP/CAT sequence flanked by *loxP* sites. Cre-mediated DNA recombination results in the removal of the EGFP/CAT sequence, followed by hVEGF-A expression (Fig. 1*Ai*, Supplemental Fig. 1*A*). Genomic DNA was isolated and amplified using PCR primers *Chi5'* (5'-GGC GGG GTT CGG CTT CTG GCG TGT GAC CGG-3') and *Veg3'* (5'-TCA CCG CCT CGG CTT GTC ACA TCT GCA AGT-3'), which recognize sequences of chicken β-actin promoter and *hVEGF-A*, respectively. In the case of hVEGF-A^{fl} mice, a 3.2-kb fragment including the EGFP/CAT and *hVEGF-A* was amplified, whereas Cre-mediated recombination in $CD19^{Cre}$/hVEGF-A^{fl} mice resulted in the amplification of a 788-bp PCR product (Fig. 1*Aii*).

LPS challenge

$CD19^{Cre}$/hVEGF-A^{fl} and $CD19^{Cre}$ mice (13 to 14 wk, $n = 5$) were injected i.p. with LPS (1 mg/kg, *Escherichia coli* 055:B5; Sigma-Aldrich, St. Louis, MO) in sterile saline prior to cytokine analysis. Blood samples were collected 8 h later by cardiac puncture. Serum was isolated from the blood samples and stored at −80°C until required.

Histopathological examination

H&E staining. Spleen and LN specimens were fixed for 24 h in 10% formaldehyde neutral buffer solution, embedded in paraffin wax, and sectioned (5–10 μm). Sections were stained with H&E.

Immunohistochemical staining

For immunohistochemistry, paraffin sections were heated in a microwave oven for 20 min, dewaxed in xylene, and rehydrated through a graded series of ethanol solutions. Endogenous peroxidase activity was blocked by incubation with 0.3% hydrogen peroxide in absolute methanol for 15 min at room temperature. Ag epitopes were heat-retrieved in Antigen Unmasking Solution (Vector Laboratories, Burlingame, CA). Samples were then incubated overnight at 4°C with primary Abs: rabbit polyclonal anti-lymphatic vessel endothelial hyaluronan receptor-1 (LYVE-1) (1/500 dilution; Upstate Biotechnology, Temecula, CA), rabbit polyclonal anti-mouse PECAM-1 (M-20) (1/500 dilution; Santa Cruz Biotechnology, Santa Cruz, CA), rat monoclonal anti-mouse CD45R/B220 (clone RA3-6B2, rat $IgG_{2a,\kappa}$, 1/50 dilution; BD Biosciences, San Jose, CA), and rat monoclonal anti-CD3 (clone CD3-12, IgG1, 1/1000 dilution; Acris Antibodies, Hiddenhausen, Germany). Primary Abs were diluted using 1% BSA in PBS containing 0.01% Tween. The incubation with the secondary Ab was carried out for 1 h using Histofine simple stain mouse MAX-PO (rabbit) or Histofine simple stain mouse MAX-PO (rat) (Nichirei, Tokyo, Japan) at room temperature. Peroxidase activity was visualized using 3,3'-diaminobenzidine (DakoCytomation, Carpinteria, CA), and the slides were lightly counterstained with Lillie-Meyer's hematoxylin (Wako, Osaka, Japan). Photographs were taken using a Zeiss Axiophot microscope with an AxioCam MRc5 camera equipped with AxioVision Release 4.6 software (Carl Zeiss, Oberkochen, Germany).

VEGF-A ELISA

Human and mouse VEGF-A level was measured in spleen homogenates and serum obtained from 13–19-wk-old $CD19^{Cre}$/hVEGF-A^{fl} and $CD19^{Cre}$ mice using Human or Mouse VEGF Immunoassay (Quantikine; R&D Systems, Minneapolis, MN) according to the manufacturer's instructions ($n = 6$).

Measurement of inflammatory cytokines

TNF-α, IFN-γ, IL-2, IL-4, and IL-5 levels were determined using a mouse Th1/Th2 Cytokine Kit (BD Biosciences). IL-1β, IL-6, and IL-10 were determined using Mouse IL-1β, Mouse IL-6, and Mouse IL-10 ELISA kits, respectively (BioSource International, Camarillo, CA). IL-9 was determined using a Mouse IL-9 ELISA Kit (RayBiotech, Norcross, GA).

Total RNA isolation and quantitative RT-PCR analysis

Total RNA was extracted from spleen, LNs, and isolated $B220^+$ and $B220^-$ cells using a total RNA isolation kit (RNAqueous, Ambion, Austin, TX). Total RNA was quantified spectrophotometrically. Total RNA (2 μg) was reverse-transcribed using the High-Capacity cDNA Reverse Transcription Kit (Applied Biosystems, Foster City, CA). Quantitative RT-PCR was performed using the TaqMan Gene Expression assay (Applied Biosystems). Reactions were run in 96-well plates in an ABI Prism 7300 Sequence Detection System (Applied Biosystems). Data collection and analysis was performed using SDSv1.4 software (Applied Biosystems), after which data were exported and further analyzed. Data were normalized based on the expression levels of GAPDH. Absence of contaminating genomic DNA was confirmed by RT-PCR of the RNA samples.

Isolation of $B220^+$ B cells

Single-cell suspensions were prepared from the spleens of 16–49-wk-old $CD19^{Cre}$/hVEGF-A^{fl} and $CD19^{Cre}$ mice by dissociation of the isolated tissues with glass slides in MACS separation buffer (Miltenyi Biotec, Bergisch Gladbach, Germany) and passage through a 30-μm nylon mesh. B cells were enriched by positive selection using CD45R (B220) microbeads and an AutoMACS Magnetic cell Sorter according to the manufacturer's instructions (Miltenyi Biotec).

Flow cytometry

Blood was collected from sevofrane-anesthetized mice by cardiac puncture and was anticoagulated with sodium citrate. Single-cell suspensions from spleen and LNs were prepared as described above. Nonspecific binding was blocked by incubation with an Fc-blocking Ab (10 μg/ml; BD Biosciences). Samples were then stained with mAbs to mouse CD4, CD8, CD19 (Beckman Coulter, Marseille, France), CD11b, CD14, and 33D1 (BD Biosciences) conjugated to PE, for 15 min at room temperature. Following surface staining, RBCs were lysed with Optilyse C (Beckman Coulter), and the remaining cells were fixed. Flow Count Beads (Beckman Coulter, Fullerton, CA) were added to the samples for quantitation. Cells were analyzed using an Epics XL flow cytometer (Beckman Coulter, Miami, FL).

OVA sensitization and challenge followed by determination of serum Ab concentration

For sensitization, 10–12-wk-old $CD19^{Cre}$/hVEGF-A^{fl} and $CD19^{Cre}$ mice were injected s.c. on day 0 with 50 μg OVA (grade V; Sigma-Aldrich) adsorbed on 100 μg (100 μl) of CFA (Sigma-Aldrich) and again on day 10 with 25 μg adsorbed on 100 μl incomplete Freund's adjuvant. Mice were challenged intranasally with 25 μg OVA in PBS on days 21, 22, and 23. Mice were killed on day 25. Serum and spleen homogenates were obtained for measurement of OVA-specific IgG1 and IgE Abs by ELISA using a mouse OVA-IgG1 and IgE kit (Shibayagi, Gunma, Japan) according to the manufacturer's instructions.

Statistical analysis

Statistical analysis was performed using the Student *t* test, Mann-Whitney's U test, or Tukey-Kramer test through all of the experimental procedures. *p* values of $*p < 0.05$ and $**p < 0.01$ were considered significant.

Results

Generation of Tg mice expressing hVEGF-A specifically in B cells

We generated mice overexpressing hVEGF-A in B cells by crossing *loxP*-flanked (floxed) EGFP mice (hVEGF-A^{fl}) onto mice expressing Cre under the control of the B cell-specific CD19 promoter ($CD19^{Cre}$) (Fig. 1*Ai*). Prerecombination, the *loxP* flanked EGFP/CAT hybrid sequence was expressed under the control of the CAG promoter, whereas the *hVEGF-A* gene was silent. Cre-mediated recombination resulted in the deletion of the EGFP/CAT sequence and subsequent expression of the *hVEGF-A* gene. This resulted in $CD19^{Cre}$/hVEGF-A^{fl} Tg mice. The *loxP* sequence, followed by *VEGF-A* sequence (Supplemental Fig. 1*A*) and the appearance of a 788-bp PCR product in the DNA from $B220^+$ cells of $CD19^{Cre}$/hVEGF-A^{fl} mice (Fig. 1*Aii*), confirmed successful recombination.

Because the *EGFP* gene is deleted from the B cells of hVEGF-A^{fl} mice during recombination to create $CD19^{Cre}$/hVEGF-A^{fl} mice, we measured the EGFP expression in $CD19^+$ B cells using flow cytometry (Fig. 1*Bi*). In $CD19^{Cre}$/hVEGF-A^{fl} mice, ~80% of the $CD19^+$ B cells were EGFP negative. This percentage was similar in $CD19^+$ B cells from spleen, LN, and blood samples (Fig. 1*Bii*). Flow cytometry using Abs against CD19, CD8, and CD4 showed that EGFP had been selectively deleted from the $CD19^+$ B cells in the $CD19^{Cre}$/hVEGF-A^{fl} mice (Supplemental Fig. 1*B*).

The expression of *hVEGF-A* mRNA was observed in spleen and LN samples from $CD19^{Cre}$/hVEGF-A^{fl} mice, but not in samples from of $CD19^{Cre}$ mice (Fig. 1*C*). The expression of *mouse VEGF-A*

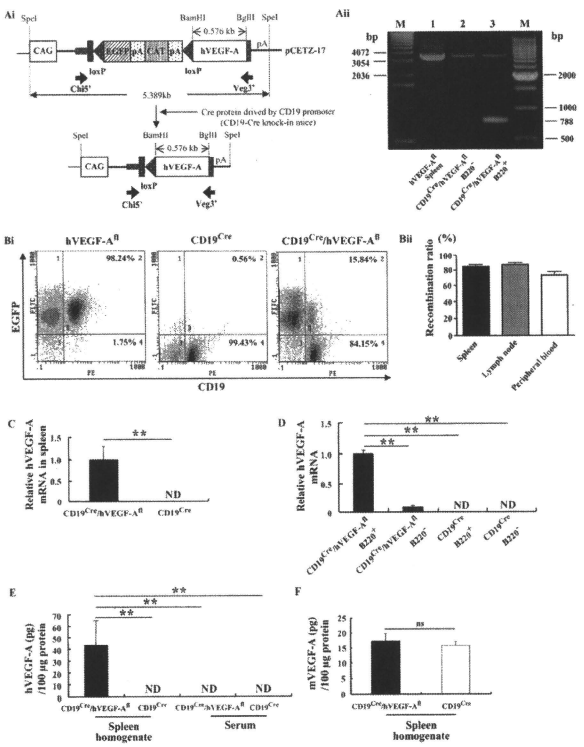

FIGURE 1. DNA constructs and Cre-mediated recombination event. *Ai*, Schematic of the target plasmid (p-hVEGF-A^{fl}) and its recombinated form are shown. *LoxP* sites are shown as triangles. The small arrows (*Chi5'* and *Veg3'*) indicate the positions and directions of the primers used for PCR. *Aii*, Identification of Cre-mediated DNA recombination product by PCR amplification of DNA isolated from spleen of hVEGF-A^{fl} mice (*lane 1*), $B220^-$ cells of $CD19^{Cre}$/hVEGF-A^{fl} mice (*lane 2*), and $B220^+$ cells of $CD19^{Cre}$/hVEGF-A^{fl} mice (*lane 3*). The 788-bp fragment represents the successfully recombinated DNA. M indicates PCR marker. *Bi*, Flow cytometry analysis of B cells from the spleen of 19–22-wk-old hVEGF-A^{fl}, $CD19^{Cre}$, and $CD19^{Cre}$/hVEGF-A^{fl} mice. Cells were stained with Abs to CD19. Percentages refer to EGFP-positive and -negative cells among $CD19^+$ cell population. *Bii*, Recombination ratio of *hVEGF-A* in the $CD19^+$ cells from spleen, LN, and blood samples. The ratio was defined as the percentage of EGFP-negative cells in the total $CD19^+$ cell population. *C*, *hVEGF-A* mRNA expression in spleen of $CD19^{Cre}$/hVEGF-A^{fl} and $CD19^{Cre}$ mice analyzed by quantitative RT-PCR ($n = 6$). *D*, *hVEGF-A* mRNA expression in $B220^+$ and $B220^-$ cells of $CD19^{Cre}$/hVEGF-A^{fl} ($n = 4$) and $CD19^{Cre}$ ($n = 5$) mice analyzed by quantitative RT-PCR. *E*, hVEGF-A protein expression in spleen homogenates and serum from $CD19^{Cre}$/hVEGF-A^{fl} and $CD19^{Cre}$ mice ($n = 6$). *F*, mVEGF-A protein expression in spleen homogenates from $CD19^{Cre}$/hVEGF-A^{fl} and $CD19^{Cre}$ mice. Data in *A–F* are representative of at least two independent experiments. $**p < 0.01$. ND, not detected.